NeuroImage 201 (2019) 116026

Contents lists available at ScienceDirect

NeuroImage

journal homepage: www.elsevier.com/locate/neuroimage

# Diffusion MRI microstructural models in the cervical spinal cord – Application, normative values, and correlations with histological analysis

Kurt G. Schilling [a,*], Samantha By [a], Haley R. Feiler [a], Bailey A. Box [a], Kristin P. O'Grady [a,d], Atlee Witt [a], Bennett A. Landman [a,b,c], Seth A. Smith [a,b,d]

[a] Vanderbilt University Institute of Imaging Science, Vanderbilt University Medical Center, Nashville, TN, USA
[b] Department of Biomedical Engineering, Vanderbilt University, Nashville, TN, USA
[c] Department of Electrical Engineering, Vanderbilt University, Nashville, TN, USA
[d] Department of Radiology and Radiological Sciences, Vanderbilt University Medical Center, Nashville, TN, USA

ARTICLE INFO

*Keywords:*
Spinal cord
Diffusion MRI
Microstructure
Validation
Multi-compartment model
Signal model

ABSTRACT

Multi-compartment tissue modeling using diffusion magnetic resonance imaging has proven valuable in the brain, offering novel indices sensitive to the tissue microstructural environment in vivo on clinical MRI scanners. However, application, characterization, and validation of these models in the spinal cord remain relatively understudied. In this study, we apply a diffusion "signal" model (diffusion tensor imaging, DTI) and two commonly implemented "microstructural" models (neurite orientation dispersion and density imaging, NODDI; spherical mean technique, SMT) in the human cervical spinal cord of twenty-one healthy controls. We first provide normative values of DTI, SMT, and NODDI indices in a number of white matter ascending and descending pathways, as well as various gray matter regions. We then aim to validate the sensitivity and specificity of these diffusion-derived contrasts by relating these measures to indices of the tissue microenvironment provided by a histological template. We find that DTI indices are sensitive to a number of microstructural features, but lack specificity. The microstructural models also show sensitivity to a number of microstructure features; however, they do not capture the specific microstructural features explicitly modelled. Although often regarded as a simple extension of the brain in the central nervous system, it may be necessary to re-envision, or specifically adapt, diffusion microstructural models for application to the human spinal cord with clinically feasible acquisitions – specifically, adjusting, adapting, and re-validating the modeling as it relates to both theory (i.e. relevant biology, assumptions, and signal regimes) and parameter estimation (for example challenges of acquisition, artifacts, and processing).

## 1. Introduction

The spinal cord (SC) acts as the primary neurological signaling conduit between the brain and the extremities as well as interfacing with the peripheral nervous system, and performs primary functions such as conducting motor information to the extremities, relaying sensory information to the brain, acting as the center for controlling various autonomic reflexes, and is also responsible for generating complex patterns such as those involved in locomotion. The SC structure consists of a central, butterfly-shaped gray matter (GM) region composed of neuronal cell bodies, dendrites, and synapses, as well as surrounding white matter (WM) tissue composed of bundles of ascending and descending axons that convey the signals between the central and peripheral nervous systems. Both the SC WM and GM are known to exhibit a range of tissue microstructural environments, with relatively large variations in axon density, size, and myelination (Saliani et al., 2017; Felten et al., 2016; Carpenter, 1991a, 1991b).

A number of neurodegenerative and immunological diseases, spinal cord pathologies, and traumatic or non-traumatic injuries can damage or affect these axons, resulting in motor and sensory deficits and a decreased quality of life. For example, inflammatory (multiple sclerosis (MS) (Stadelmann, 2011; De Santiset al., 2018), transverse myelitis (Krishnan et al., 2006)), degenerative (amyotrophic lateral sclerosis (Kawamata et al., 1992), Friedreich's ataxia (Cheviset al., 2013; Mascalchi et al., 1994)), developmental (cerebral palsy (Kuczynskiet al., 2017; Clowry, 2007), spina bifida (Hasan et al., 2008)), and orthopedic (stenosis (Martinet al., 2018)) disorders, as well as injury (Chen et al., 2015;

* Corresponding author.
*E-mail address:* kurt.g.schilling.1@vumc.org (K.G. Schilling).

https://doi.org/10.1016/j.neuroimage.2019.116026
Received 1 March 2019; Received in revised form 12 July 2019; Accepted 16 July 2019
Available online 19 July 2019

**Abbreviations**

| | |
|---|---|
| SC | spinal cord |
| GM | gray matter |
| WM | white matter |
| DTI | diffusion tensor imaging |
| NODDI | neurite orientation dispersion and density imaging |
| SMT | spherical mean technique |
| CSF | cerebrospinal fluid |
| FA | fractional anisotropy |
| MD | mean diffusivity |
| AD | axial diffusivity |
| RD | radial diffusivity |
| FISO | isotropic volume fraction |
| FICVF | intra-cellular volume fraction |
| ODI | orientation dispersion index |
| INTRA | intra-neurite volume fraction |
| DIFF | intrinsic diffusivity |
| EXTRA-TRANS | extra-neurite transverse diffusivity |
| EXTRA-MD | extra-neurite mean diffusivity |
| ROI | regions of interest |

Guoet al., 2019) and tumors (Clauset al., 2010), are known to lead to changes in spinal cord microstructure, including demyelination, edema, axonal loss, reduced axon integrity, or axonal reorganization. Thus, characterizing the SC microstructure can serve an important role in diagnosis and prognosis of these pathologies, as well as lead to a better understanding of disease pathophysiology, functional impairment, or treatment efficacy.

Towards this end, non-invasive biomarkers based on quantitative magnetic resonance imaging (MRI) have shown potential for characterizing SC microstructure (Smith et al., 2014; Lemaet al., 2017; Levyet al., 2018; Battistonet al., 2018; Samsonet al., 2013; Ljungberget al., 2017; Duvalet al., 2017; Dula et al., 2010; Harkins et al., 2012; Harkins et al., 2013). In particular, diffusion MRI (dMRI) shows promise for non-invasively characterizing tissue micro-environments. To date, the most readily available diffusion MRI technique (in both the brain and spinal cord) is diffusion tensor imaging (DTI) (Basser et al., 1994), which represents the diffusion of water in tissue as a 3D Gaussian distribution. DTI provides quantitative indices such as fractional anisotropy (FA), mean diffusivity (MD), axial diffusivity (AD), and radial diffusivity (RD) (Pierpaoli et al., 1996; Basser and Pierpaolieng, 1996) which have been shown to be sensitive to SC tissue properties (Budde et al., 2009; Klawiteret al., 2011; Songet al., 2005), such as axon density, axonal injury, and degree of myelination. While DTI is sensitive to a number of microstructural features, it lacks the specificity to disentangle precise microstructural changes.

As an alternative to "signal" models (i.e., DTI), recent years have seen a proliferation of techniques - termed "microstructural" or "multi-compartment" models - which explicitly model certain aspects of the tissue environment (Feriziet al., 2015; Panagiotaki et al., 2012; Assaf and Basser, 2005; Assaf et al., 2008; Novikov et al., 2018a; Landman et al., 2010). Two of the more commonly implemented (and clinically feasible) microstructural models to date are the Neurite Orientation Dispersion and Density Imaging (NODDI) technique (Zhang et al., 2012) and the Spherical Mean Technique (SMT) (Kaden et al., 2016). The NODDI model represents the signal in each voxel as the sum of three tissue compartments – intra-cellular, extra-cellular, and CSF compartments. The intra-cellular compartment is composed of neurites (modelled as zero-radius sticks) with a distribution of directions (i.e. a bipolar symmetric Watson distribution) that includes both an average direction and a spread of orientations around that direction. Thus, application of NODDI results in the isotropic (or CSF) volume fraction (FISO), the intra-cellular volume fraction (FICVF), and an orientation dispersion index (ODI) where a higher value represents a larger spread of axon orientations. SMT uses a two-compartment model that estimates microscopic features specific to the intra- and extra-neurite compartments un-confounded by the effects of fiber orientation and their distributions, by modeling the intra-neurite compartment as zero-radius sticks, and the extra-neurite tissue as a symmetric tensor. This technique results in an intra-neurite volume fraction (INTRA), a tissue intrinsic diffusivity (DIFF), and diffusivities of the (potentially) anisotropic extra-neurite compartment including its transverse microscopic diffusivity (EXTRA-TRANS) and mean diffusivity (EXTRA-MD).

Several microstructural models were originally applied to and validated within the spinal cord (Assaf et al., 2000, 2008; Ong and Wehrlieng, 2010), due to its rather coherent white matter orientations, making it an ideal model for validation. However, many tissue models, including both NODDI and SMT, were developed for, and are largely applied to, the brain (Metzler-Baddeleyet al., 2019; Li et al., 2019; Pietschet al., 2019; Spanoet al., 2018; Kadotaet al., 2018; Masjoodi et al., 2018; Sone et al., 2018; Araque Caballeroet al., 2018; Schilling et al., 2018; Parvathaneniet al., 2018; Li et al., 2018; Kamiyaet al., 2018). While application of multi-compartment models in the SC is limited, several studies have demonstrated feasibility and potential clinical utility of these techniques. For example, Grussu et al. (2015) characterize WM and GM NODDI contrast, demonstrate superior fitting and reproducibility of NODDI metrics in comparison to DTI, and validate NODDI ODI index in characterizing MS lesions (Grussuet al., 2017). In parallel, By et al. (2017) observed a decrease in FICVF in MS lesions and superior WM/GM contrast compared to DTI. Additionally, By et al. (2018) implemented SMT in the same subjects, characterizing normal WM and GM indices, and demonstrating abnormal compartmental diffusivities in normal appearing WM of MS patients. Together, these studies suggest that the contrast provided by these models may offer useful, clinically feasible, outcomes that offer unique insight into the SC microstructure.

One limitation of clinically feasible diffusion microstructural modeling of the in vivo human SC is that currently they provide global characterization of WM and GM indices. However, these models have been unexplored in as to whether they provide contrast among the various SC pathways and regions where heterogeneous axonal environments are expected (we note several exceptions in animal models (Assaf et al., 2008; Ong and Wehrlieng, 2010) or using advanced hardware (Duvalet al., 2015)). Thus, the first aim of the current study is to investigate WM and GM sub-regions of the SC and provide tissue- and column-specific normative values of both the signal models (DTI) and clinically achievable microstructural models (NODDI, SMT). We do this by analyzing twenty-one healthy subjects, in a standard space, and performing simple region-of-interest analysis. This aim is made possible by recent advancements in SC analysis and processing tools (i.e. the Spinal Cord Toolbox (De Leeneret al., 2017)) as well as the creation of a standard space SC atlas and templates (De Leener et al., 2018) with integrated WM pathways and GM regions of interest (ROI).

While characterization of normative values is important, it is also necessary to properly validate potential biomarkers against ground truth measures of microstructure. Thus, our second aim is to validate sensitivity and specificity of these models. Validation can be performed against numerical or physical phantoms (Dyrby et al., 2018; Fanet al., 2018; Schillinget al., 2018a; Hubbard et al., 2014; Fieremans and Lee, 2018; Fieremans et al., 2008); however, it is hard to replicate the enormous complexity and exact microstructural environments of the SC. Alternatively, comparisons against known anatomy (through histological analysis) can be made (Schilling et al., 2018; Schilling et al., 2016; Seehauset al., 2015; Budde and Annese, 2013; Budde and Frank, 2012; Leergaardet al., 2010; Dyrby et al., 2012; Alexanderet al., 2010). Knowledge about SC WM and GM composition is an accumulation of decades of research by neuroanatomists (see Saliani et al. for a review (Saliani et al., 2017)). Most cyto- and myelo-architecture is described qualitatively, with microstructural metrics measured quantitatively in

only specific tracts (most commonly the corticospinal and pyramidal tracts) and often using different methodologies – making comparisons across sub-regions difficult. However, recently Duval et al. (Duvalet al., 2019) have imaged a fixed human spinal cord using high resolution scanning electron microscopy from C1 to L5 spinal levels, quantifying morphometric features across the entire cord (including both WM and GM) and essentially creating a "microstructural" template of the human spinal cord. Fortuitously, Duval et al. (Duvalet al., 2019), also register this to the same PAM50 template space in which we provide normative dMRI values, facilitating comparison of these values to expected trends observed in histological analysis.

This manuscript is organized as follows. We first describe methodologies related to image acquisition, processing, and alignment to standard space which facilitates quantification of dMRI-derived metrics in WM and GM, as well as in a number of SC sub-regions. We show qualitatively what these measures look like in the healthy human SC, and describe normative values in each ROI. Finally, we compare these measures to that expected from histological analysis and calculate correlation coefficients for all dMRI-estimated features against all histological microstructure features.

## 2. Methods

### 2.1. MRI experiments

Twenty-one healthy controls participated in this study. All experiments were performed on a 3.0T whole body MR scanner (Philips Achieva, Best, Netherlands). A two-channel body coil was used for excitation and a 16-channel SENSE neurovascular coil was used for reception. The maximum gradient strength of the system was 80 mT/m at a slew rate of 100 mT/m/s. All data were acquired under a protocol approved by the local institutional review board and signed, informed consent was obtained prior to the study.

For each subject, a high-resolution ($0.65 \times 0.65 \times 5\ mm^3$) multi-slice, multi-echo gradient echo (mFFE) anatomical image (Held et al., 2003) was acquired (TR/TE/ΔTE = 753/7.1/8.8 ms, $\alpha = 28^\circ$, number of slices = 14, 6:12 min) for co-registration and to serve as a reference image for segmentation. The diffusion sequence consisted of a cardiac-triggered (using a peripheral pulse oximeter with a delay set to 127 ms), spin echo sequence with single-shot echo planar imaging (EPI) readout with the following parameters: TR/TE = 5 beats (~3000 ms)/65 ms, resolution = $1.25 \times 1.25\ mm^2$, slice thickness = 5 mm, FOV = $68 \times 52$ mm, SENSE (AP) = 1.5 and NEX = 3, number of slices ranged from 1 to 5 as the study progressed. Importantly, all images were centered on the C3 level and the middle slice of each was used for analysis. Reduced field-of-view was applied using an outer volume suppression technique (Wilm et al., 2007) and fat suppression was achieved using SPIR. A multi-shell acquisition, similar to the previously published NODDI protocol in the brain (Zhang et al., 2012) and the one implemented in the spinal cord (Grussu et al., 2015) was used with uniform sampling: (i) $b = 711\ s/mm^2$ with 32 directions and (ii) $b = 2855\ s/mm^2$ with 64 directions, with constant gradient times of Δ (separation between gradients) = 31.8 ms and δ (gradient duration) = 21.0 ms. A non-diffusion weighted scan ($b = 0\ s/mm^2$ or b0) was acquired with each shell. Total scan time was 18:11 min. Images were acquired in the axial plane for both the anatomical and diffusion images. SNR in the b0 images was found to be approximately 30 across the entire cord where noise was defined using the standard deviation of the difference of two measurements.

### 2.2. Image processing and diffusion MRI-derived measures

A pipeline similar to the template-based analysis pipeline implemented in the SCT (De Leeneret al., 2017) was utilized. SCT diffusion MRI motion correction was performed (Xuet al., 2013), followed by registration of the b0 image to template space. Registration was assisted by segmentation of the spinal cord and vertebral labeling (i.e. designating that the slice is centered on C3) and performed in three steps: affine registration of the segmentation as initialization, affine registration of the b0 using a mean squares cost function, and finally a non-linear symmetric normalization algorithm. The resulting warp field was applied to all scalar quantitative diffusion MRI metrics (detailed below), resulting in all measures aligned with the PAM50 WM and GM labels, and the WM and GM tissue- and column-specific labels, as well as aligned with the histological template (Duvalet al., 2019).

NODDI fitting was performed using the NODDI MATLAB Toolbox (https://www.nitrc.org/projects/noddi_toolbox). Diffusion coefficients for the intra-axonal and isotropic compartments were fixed with values of 1.7 $\mu m^2/ms$ and 3.0 $\mu m^2/ms$ respectively as in (Zhang et al., 2012). As described in the introduction, after fitting the derived NODDI indices included: the isotropic volume fraction (FISO) representing the fraction of free water such as CSF, the apparent intra-cellular volume fraction (FICVF) representing the fraction of dendrites and axons, and an orientation dispersion index (ODI) a measure of how axons disperse around a central orientation.

SMT fitting to the diffusion-weighted data was performed using C++ code provided by the authors of (Kaden et al., 2016) (https://github.com/ekaden/smt). SMT fitting yielded maps of the apparent intra-axonal volume fraction (INTRA), the intrinsic diffusivity (DIFF), and the diffusivities associated with the extra-axonal compartment including the transverse (EXTRA-TRANS) and mean diffusivity (EXTRA-MD).

Finally, in contrast to microstructural models, the conventional DTI analysis (i.e. a signal model) was also performed using a non-linear fit in Camino utilizing both shells, resulting in fractional anisotropy (FA), mean diffusivity (MD), axial diffusivity (AD), and radial diffusivity (RD) indices.

### 2.3. Quantitative analysis

#### 2.3.1. WM and GM comparison

To reproduce previous results characterizing indices over the full WM and GM ROIs, we calculated the medians of each derived index within both WM and GM. A nonparametric Wilcoxon rank sum test was performed for each index to probe statistically significant differences and discriminatory power of contrasts.

#### 2.3.2. ROI-based normative values

To assess normative values in the tissue and column labels, we utilized those in the PAM50 template. In our data, this includes 33 labels (ROI names and abbreviations are given in the appendix), including 6 GM regions, 26 WM regions, and the CSF contour. For ease of visualization in boxplots, the WM can be hierarchically grouped into dorsal columns (4 labels), lateral funiculi (8 labels), and ventral funiculi (14 labels). We note that variations in microstructural environments are expected even within this hierarchical grouping.

#### 2.3.3. Correlation with histological template

Finally, we related the median derived contrasts from DTI, NODDI, and SMT across all subjects to the ROI-median microstructural values provided in the histological template. The histological template includes axon diameter (μm), myelin volume fraction (%), axon volume fraction (%), the number of axons (axons/100 $\mu m^2$), and the density of axons (axons/100 $\mu m^2$) with a size range of 1–4 μm and with a larger size of 4–8 μm. Pearson's linear correlation coefficients were determined between the diffusion-derived parameters and histological measures, with the two-tailed Student's t-distribution used to determine statistical significance of correlations. We note that for extraction of ROI-based normative values and correlation of histological template a weighted average metric extraction (Lévy et al., 2015) was utilized to attempt to account for possible partial volume effects, with similar (although not the same) results when using a simple binary average metric extraction.

## 3. Results

### 3.1. Anatomy and template

Fig. 1 illustrates the ascending and descending WM pathways, as well as GM ROIs separated based on cytoarchitectural features, and is the standard diagram used to depict SC anatomy (figure illustrated by Frank H. Netter, and reproduced and adapted from Netter's Atlas of Neuroscience, with permission from Elsevier). For comparison, Fig. 2 (top) displays the T2* contrast from the SC template, as well as labels, which correspond well spatially to those from expected anatomy, although limited to a coarse spatial resolution defined by MRI.

Additionally, Fig. 2 (bottom) displays the microstructural metrics extracted from the SEM-derived histological template. A delineation of WM and GM is clear, with GM consisting of microenvironments with smaller axon diameters, axon densities (of all sizes), axon volume fractions, and myelinated volume fractions. Notably, and as described by Duval et al. (Duvalet al., 2019), several trends are also apparent across the WM pathways, revealing a somatotopic and/or functional organization (Niuet al.eng, 2013). For example, contrast between the fasciculus cuneatus and gracilis sensory axons originating from different parts of the body (i.e., arms and legs, respectively) (Niuet al.eng, 2013) clearly shows an increased diameter, volume fraction, and myelin content of the cuneatus. Areas of high density small axons include many of the descending ventral funiculi (vCST, TST, vRST, lVST), while the spinocerebellar tract generally consists of large, myelinated axons. Thus, while not perfectly delineated by the atlas labels, key morphological differences are apparent.

### 3.2. Qualitative comparisons

Figs. 3–5 show montage diffusion-derived maps for all 21 subjects for DTI, NODDI, and SMT, respectively. Note that the gray-scale background of each image is the individual subject's non-diffusion weighted image, highlighting quality template normalization for all subjects. Most notable differences in contrast are observed between WM and GM, which are generally distinguishable in the DTI AD, FA, RD maps, the NODDI ODI map (which indicates high dispersion particularly in the ventral horns), and is somewhat distinguishable in the SMT DIFF and INTRA maps for several subjects. Interestingly, the DTI parametric maps are generally consistent across subjects, while there is some variation in scale and spatial patterns derived from the microstructural models.

### 3.3. Normative values

The subject-averaged parametric maps in template space are shown in Fig. 6. After averaging, spatial trends are apparent. DTI values tend to separate WM from GM. NODDI ODI clearly highlights the ventral horn and intermediate zones, and the dorsal horn to a lesser extent. FISO and FICVF show distinct patterns that do not necessarily follow the WM/GM boundaries. One clear feature near the left and right lateral corticospinal tracts is an increase in FISO and FICVF (white arrows). This unique, symmetrical feature is also apparent as high indices for all SMT metrics. SMT and NODDI qualitatively show similar boundaries or organization of spatial patterns, again not limited to highlighting WM/GM contrast.

Quantitative WM and GM comparisons agree with qualitative results, as well as past quantitative SC diffusion studies (Grussu et al., 2015; By et al., 2017; By et al., 2018; Byet al., 2016), with boxplots of the median value for all subjects shown in Fig. 7. As in (Grussu et al., 2015), DTI shows an increased AD, increased FA, increased MD, and decreased RD in WM compared to GM. Similarly, NODDI indicates a decreased ODI and increased FISO (Grussu et al., 2015), although we found no significant difference in FICVF. A direct comparison with (By et al., 2018) is not possible because control WM was only compared to MS normal appearing WM, but we find significantly increased DIFF and EXTRA-MD in WM compared to GM.

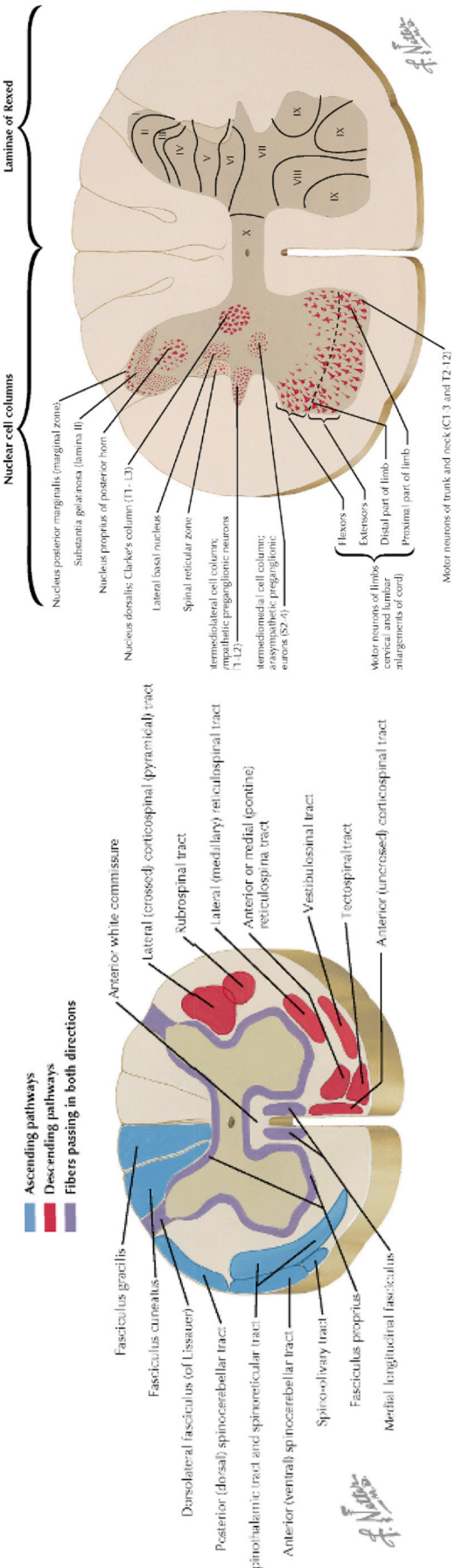


**Fig. 1.** Spinal cord cross sectional anatomy. Illustration of the principal WM fiber tracts of the spinal cord (left) and GM ROIs and architectural features (right) are shown for a cross-section through the cord. Note that figure is only for educational purposes (and in our case, to orient reader to spinal cord anatomy) of white and gray matter regions and is not illustrative of one specific spinal cord level. Figures illustrated by Frank H. Netter, and reproduced and adapted from (Felten et al., 2010) with permission from Elsevier.

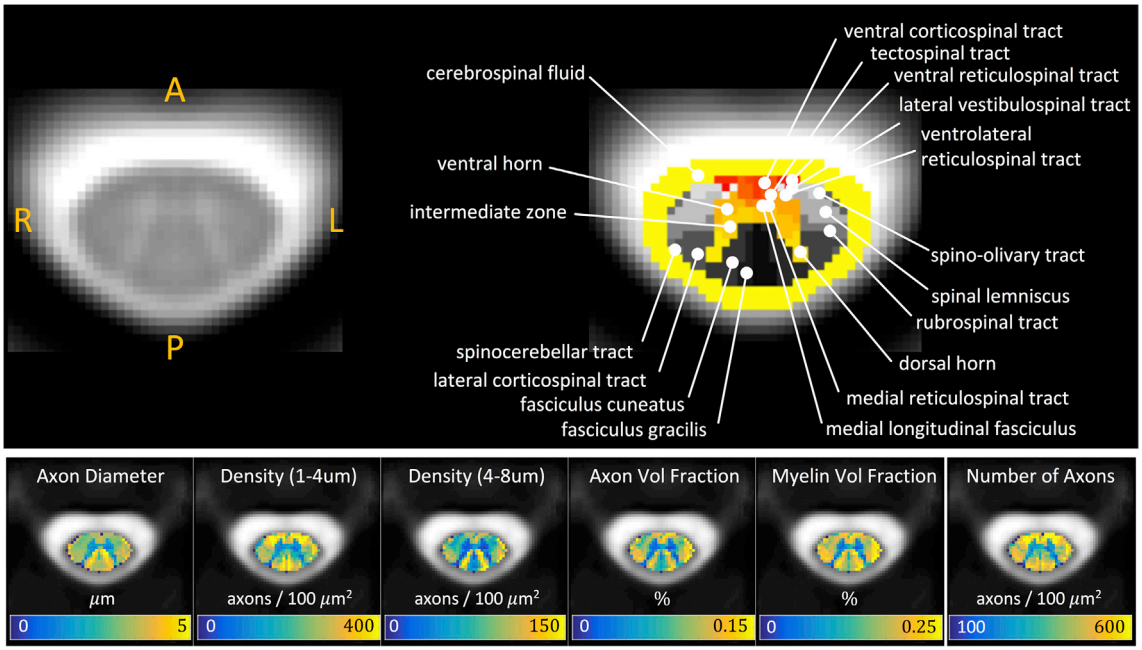


**Fig. 2.** PAM50 T2* template at the C3 vertebral level with WM pathways and GM subdivisions (top) and histological template of tissue microstructure indices (bottom). Note that histological indices were down-sampled to native atlas resolution.

We next probe whether these metrics show contrast across heterogeneous WM pathways and GM sub-divisions. Figs. 8–10 show normative values over all subjects, across all 33 anatomical locations, for DTI, NODDI, and SMT, respectively. Note that vertical lines subdivide dorsal column labels, lateral funiculi, ventral funiculi, GM, and CSF for ease of viewing, although we may not expect the same values within or across regions. It is clear that there is significant variation across both WM and GM (and expected extreme values for CSF) for all metrics from all models. Inspection of inter-quartile range, which gives an indication of inter-subject variability, indicates that DTI measures are more reproducible across subjects, while those of the more complex models generally show increased inter-subject variability. For all models, larger variation is observable in the ventral funiculi regions, which are generally smaller in size (i.e., prone to possible partial volume effects) than other white matter regions. We next ask whether these metrics follow expected histological trends.

### 3.4. Comparisons and correlations with histology

Figs. 11–13 show plots of the diffusion-derived indices plotted against histological measures for DTI, NODDI, and SMT, respectively. Correlation coefficients are indicated on each plot, with significance indicated by asterisks (and BOLD outline surrounding plot). We note that these plots include both WM and GM ROIs (they exclude CSF). Diffusion and histological correlations in WM only are given as Supplementary Figs. 1, 2, and 3 (for DTI, NODDI, and SMT, respectively) which indicate that some, but not all, of the correlations described below are driven by differences between WM and GM. Because these tissue and signal models estimate features that inherently exist in both white and gray matter (i.e., diffusivities, dispersion, and volume fractions), we chose to include the plots that validate microstructure of both tissue types in the main body of the manuscript.

As expected (Budde et al., 2009; Klawiteret al., 2011; Songet al., 2005), DTI (Fig. 11) is sensitive to nearly all microstructural features. For example, intuitively, RD decreases with an increased axonal volume fraction, increased axonal density (of all axons), and increased myelination, while FA increases under the same conditions. However, we note that most DTI correlations are driven by global differences in white and gray matter, rather than distinguishing white matter microstructure alone (see Supplementary Fig. 1).

Similarly, NODDI (Fig. 12) exhibited intuitive correlations. For example, isotropic volume fraction decreased with increasing densities of microstructural tissue (increasing densities, increasing axon and myelin volume fractions) although correlations were not as significant as DTI. However, FICVF, intended specifically to be a surrogate marker of axon volume fraction, did not significantly vary with this index. Additionally, ODI varied with diameter, density of larger axons, AVF and MVF, although none of these are measures of tissue orientation. Like DTI metrics, The FICVF and ODI trends described above are largely driven by the large dynamic range provided by including gray matter in the analysis (see Supplementary Fig. 2).

SMT (Fig. 13) showed most sensitivity to axonal diameter with an increasing diameter resulting in increased intracellular volume fraction and decrease extra-neurite diffusivities (similar trends are observed in WM analysis alone, although no longer statistically significant – see Supplementary Fig. 3). While the intracellular volume fraction did positively correlate with the axon volume fraction, the correlation was small. Further, intracellular volume fraction and axon volume fraction correlation was non-existent when analyzing WM ROIs alone (see Supplementary Fig. 3).

## 4. Discussion

Often, in the diffusion literature, the spinal cord is assumed to be an extension of the brain, with a much-simplified geometry. In fact, due to its mostly parallel fiber orientations, it has served as the model of choice (Jelescu and Budde, 2017) for assessing anisotropy in the central nervous system (Schwartzet al., 2005; DeBoyet al., 2007), demonstrating performance of microstructure or geometric models (Assaf et al., 2000; Skinner et al., 2017), or studying diffusion time effects (Nossin-Manor et al., 2002; Biton et al., 2006, 2007; Jespersen et al., 2018). Here, however, we find that microstructural models created for the brain (and demonstrated to be quite useful for understanding normal and abnormal development and diseases) are not as strongly associated with the histological values they intend to recover (and sometimes explicitly model). In fact, the spinal cord may be one of the more simple neurological structures with which to validate models due to minimal confounds such as crossing fibers or large orientation dispersions yet has somatotopic

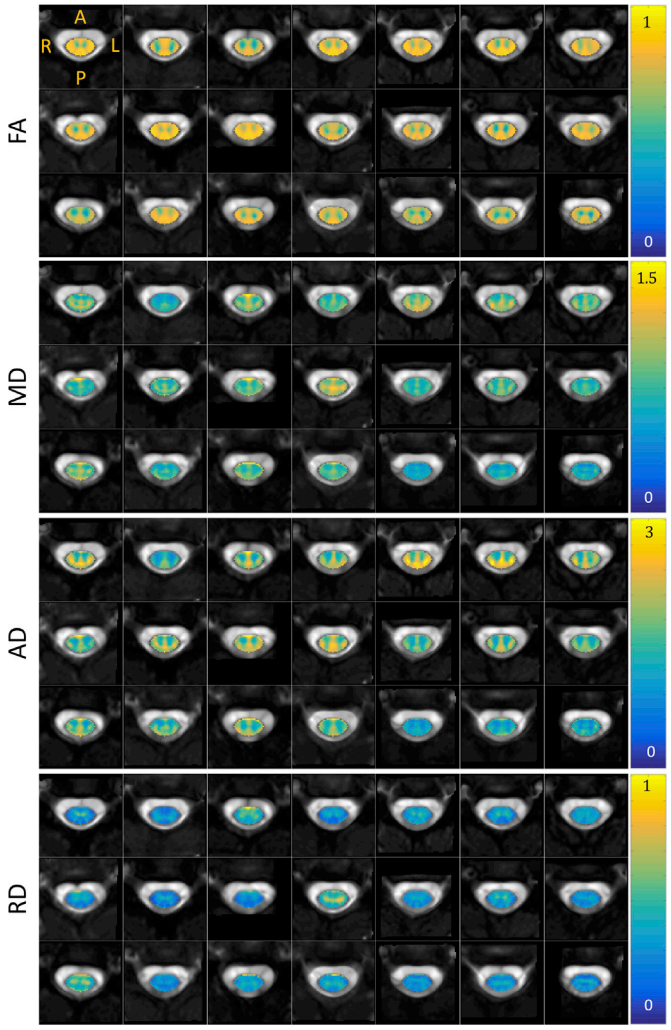


**Fig. 3.** Montage of DTI metrics (fractional anisotropy, mean diffusivity, axial diffusivity, and radial diffusivity) for all subjects in atlas space. Diffusivity in units of $10^{-3}$ $mm^2/s$. Note that each axial view corresponds to a different subject at the C3 vertebral level in atlas space.

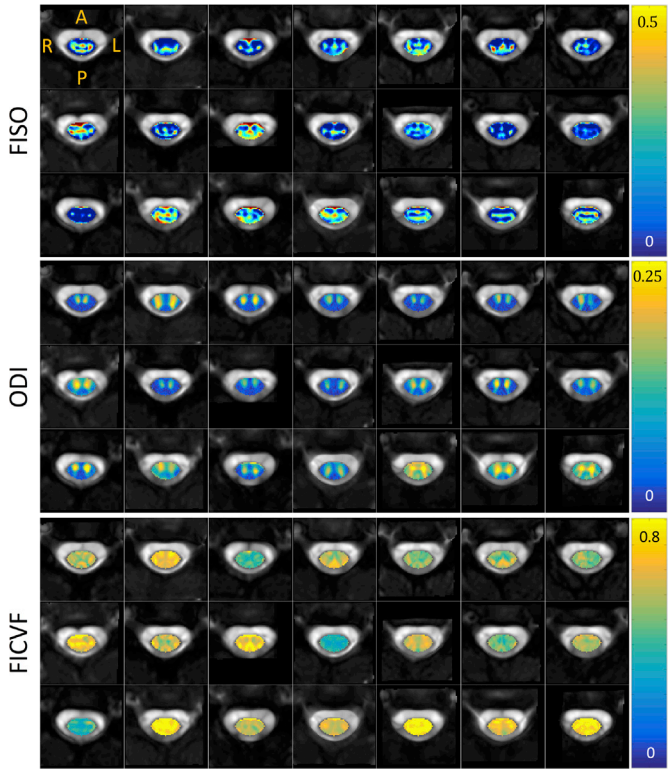


**Fig. 4.** Montage of NODDI metrics (isotropic volume fraction, orientation dispersion index, intracellular volume fraction) for all subjects in atlas space. Note that each axial view corresponds to a different subject at the C3 vertebral level in atlas space.

organization. While this may seem like a relatively cynical view of these results, it is important to emphasize that these models still show strong sensitivity to various microstructural features relevant to a number of diseases and disorders, which have already proven to be potentially relevant markers of pathology (Grussuet al., 2017). Thus, although these "models" may not provide absolute interpretations of the tissue microstructure, they are still both practical and valuable (Novikov et al., 2018b). However, it may be necessary to re-envision multi-compartment diffusion models and improved acquisitions for spinal cord architecture in order to exactly determine the tissue parameters of interest with high sensitivity and specificity.

For example, these models are not exempt from limiting assumptions and consequent biases. An example is the fixed diffusivity assumption and representation of distributions as a specific distribution in NODDI (both of which SMT is ideally unaffected by) (Jelescu et al., 2015), or the assumption of a discrete number of compartments (both studied models incorporate this, although others do not (Wanget al., 2011; Scherrer et al., 2016)), or assumptions on diffusivity profiles or differences/similarities of intra and extra-cellular diffusivities (Lee et al., 2018). Many of these assumptions can possibly be better adapted for the spinal cord. Possibly by utilizing prior knowledge of expected fiber orientation (at least in WM regions), largely parallel single fiber populations, or expected axonal diameters (which show greater variation of smaller spatial scales than that of the brain). Acquisition can additionally be optimized using similar prior information (Schillinget al., 2018b) (i.e. images acquired with diffusion weighting in the direction of axons are at or near the noise floor).

While the multi-compartment models show limited correlations with histology, the model itself may not be the sole source of the problem. Rather, the model *in combination with* analysis and acquisition may be the limiting factor. SC imaging is inherently noisy, susceptible to a number of artifacts, and a community consensus is lacking on acquisitions, analysis tools, and processing pipelines. Thus, partial-volume effects, subject-to-template registration, Gibbs ringing, susceptibility distortions, the relationship between cardiac triggering and CSF pulsation, and metric extraction all likely play a role in the limited microstructural sensitivity and specificity. However, our study was performed using a clinically acceptable acquisition (one which has been shown to be adequate for brain multi-compartment imaging) with pre-processing, processing, and analysis pipelines that are commonly applied (and are arguably the current state-of-the-art) in the in vivo human SC literature (Guoet al., 2019; Grussu et al., 2015; By et al., 2017; Duvalet al., 2015; De Leeneret al., 2017; De Leener et al., 2018; Lévy et al., 2015; Byet al., 2016; Cohen-Adad, 2018; Grussuet al., 2016). Thus, there are limitations when using these multi-compartment models, in combination with standard clinical imaging protocols and open-sourced processing pipelines, and improvements in any or all of these areas are needed for accurate and precise SC tissue quantification in a clinically feasible scan. All aspects of the analysis should be carefully considered when designing diffusion studies of the cord, and we should be mindful of these potential shortcomings and how it affects what we study.

As described by Novikov et al. (2018b) modeling involves both theory *and* parameter estimation. In this study, while we cannot explicitly define the lack of sensitivity and specificity to either of these individually, our results suggest that "modeling" these microstructural measures

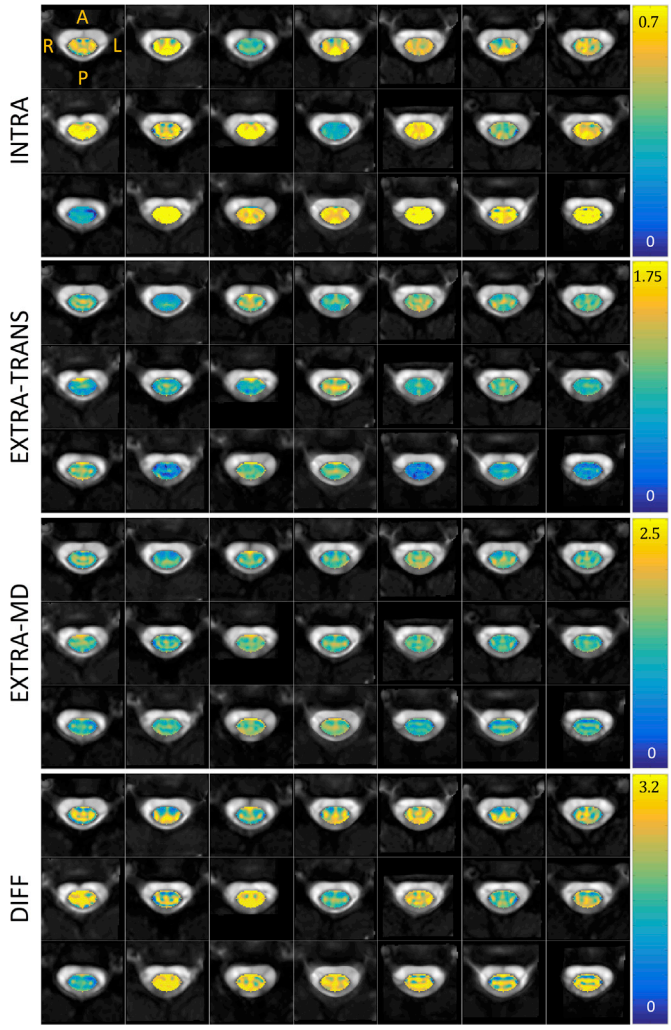


**Fig. 5.** Montage of SMT metrics (intra-neurite volume fraction, extra-neurite transverse microscopic diffusivity, extra-neurite mean diffusivity, and tissue intrinsic diffusivity) for all subjects in atlas space. Diffusivity in units of $10^{-3}$ mm$^2$/s. Note that each axial view corresponds to a different subject at the C3 vertebral level in atlas space.

(specifically axon volume fractio) in the spinal cord on clinical-quality datasets is not able to recover expected spatial trends in microstructure in the individual (or population averaged) cord. As described above, these limitations are likely a combination of both theory (i.e., the framework and assumptions of the model) and parameter estimation (inherently affected by image quality, image acquisition, and artifacts).

Although several tissue model parameters were indeed sensitive to microstructural indices, much of the strong correlation was driven by differences and the heteroscedasticity of variables between WM and GM. The variability between the two tissue types is greater than the variability between them, resulting in a large dynamic range (of both histology and diffusion metrics) and a strong correlation. However, within a tissue type (i.e., the WM), the variability between sub-regions is smaller than that detectable by the multi-compartment models and correlations are no longer apparent (see next paragraph on possible contributions to the low detectability of models in the SC). Although not broadly discussed, this is a common result in the literature. For example, when comparing an index between two populations (i.e., healthy and diseased) strong correlations may be present which are driven by the large dynamic range presented by the two populations together. This, in itself, doesn't make the metric less valuable, as a strong effect size (i.e. Cohen's d) can certainly result in a useful biomarker, even if biological interpretation is unclear or imprecise.

There are a number of modeling approaches and strategies not evaluated in this study due to relevant scan time or gradient strength limitations. For a time, spinal cord diffusion imaging was limited by motion, pulsatile flow artifacts, susceptibility artifacts, and the size of the cord (Wheeler-Kingshottet al., 2002) in addition to lack of SC specific tools for pre-processing. However, with advances in acquisition, tools (De Leeneret al., 2017), and templates (De Leener et al., 2018), in parallel with advances in microscopy (Duvalet al., 2019; Cohen-Adad, 2018), clinically feasible application and validation of these techniques is likely to increase in the future (Assaf et al., 2008; Alexanderet al., 2010; Benjamini et al., 2016; Xuet al., 2016; Xuet al., 2014; Dyrby et al., 2013; Westinet al., 2016). These may prove more sensitive to a number of indices.

Adding more contrasts, possibly in combination with diffusion data, may provide more sensitive and specific measures of SC microstructure. For example, magnetization transfer or quantitative magnetization transfer (Smith et al., 2014; Dula et al., 2010; Reichet al., 2007), g-ratio mapping (Duvalet al., 2017; Duval et al., 2018), or T1w/T2w imaging (Ganzetti et al., 2014) may better quantify the myelin volume fraction (which diffusion is blind to) thereby improving estimates of the additional compartment sizes. Additionally, standard relaxometry (Harkins et al., 2012, 2013) can be combined with diffusion to gain insights into local tissue volumes or physiological environments. Finally, post-processing of diffusion data using fiber tractography may enable the ability to distinguish SC environments through tract density images (Calamante et al., 2010), streamline clustering (Garyfallidiset al., 2018), or connectivity profiles (Fujiyoshiet al., 2013). As both diffusion and non-diffusion techniques become clinically viable, future in vivo human validation should be performed against prior anatomical knowledge or histological templates as in the current study.

### 4.1. Observations

While the brain and spinal cord share many of the same structures on the scale of microns (i.e. neurites, axons), they can vary dramatically in the scale of bundles of axons. For example, the pathways in the brain (e.g. the corpus callosum, internal capsule) can be as wide as multiple centimeters in diameter, whereas the entire spinal cord (and all associated pathways) is on the order of a single centimeter. Thus, the pathways we measure in this study are of a much finer scale than is typical in the brain. Although our in-plane resolution is higher than typical brain acquisitions (usually 2–2.5 mm isotropic), many of the WM tracts analyzed occupy very few voxels (Fig. 2), and partial volume effects are almost certain to occur (see *Limitations* section). Future microstructural models may incorporate not only multiple compartments with varying diffusivities, but multiple compartments of the same matter (i.e. multiple extracellular compartments) that also can vary in diffusivities.

Looking at the montage images (Figs. 3–5) and subject-average templates (Fig. 6) gives insight into potential limitations of some aspects of each model. DTI shows consistent indices, across all subjects, for all measures, and WM/GM boundaries are clearly delineated. These results are confirmed by significant differences in all metrics between WM and GM (Fig. 7) for DTI. However, SMT and NODDI have some measures that vary greatly across subjects, in particular INTRA for SMT and FISO for NODDI. The FISO can possibly be explained by the fixed intrinsic diffusivity (which we see does indeed vary across and within subjects based on SMT DIFF values), causing estimates of FISO (which represents the compartment fraction with that fixed diffusivity) to increase/decrease unexpectedly. However, the other measures from these models show consistent patterns. Interestingly, these patterns do not always follow the WM/GM boundaries (with the exception of NODDI ODI). The templates show a unique "cheek-like" feature, near the left and right CST, which are expected to have high numbers of heavily myelinated large fibers (see Fig. 2). Although boundaries between regions are not clearly

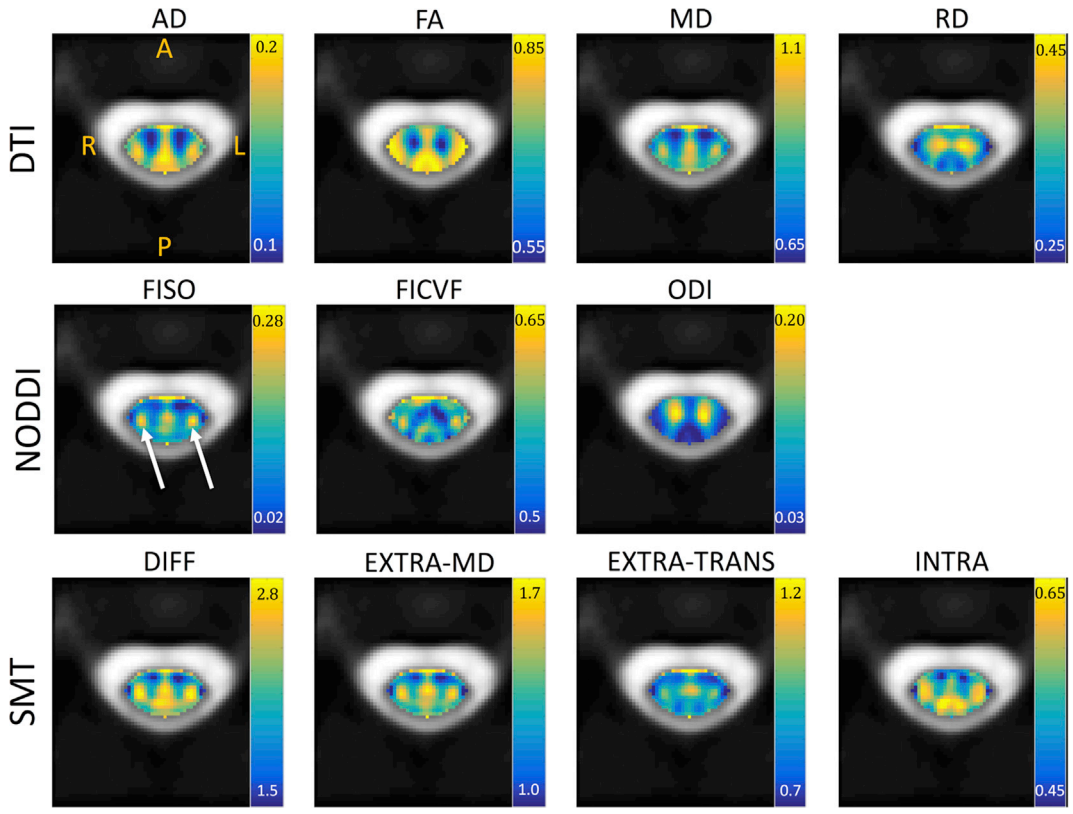


**Fig. 6.** Metrics averaged over all subjects in atlas space. Diffusivity in units of $10^{-3}$ $mm^2/s$.

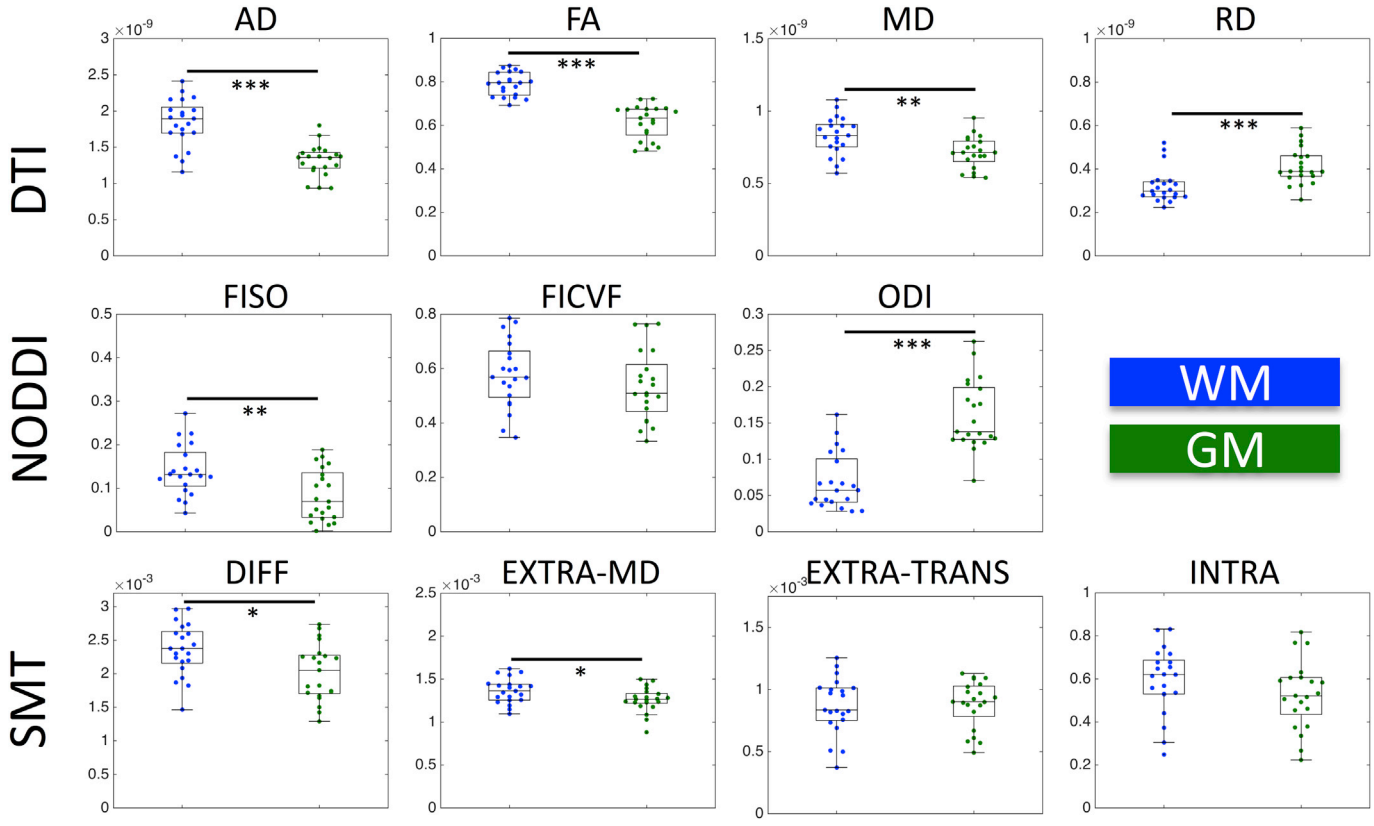


**Fig. 7.** Medians of DTI, NODDI, and SMT metrics within WM (blue) and GM (green). Statistical significance is determined by a nonparametric Wilcoxon rank sum test and is indicated by asterisks (*p < 0.05; **p < 0.01; ***p < 0.001).

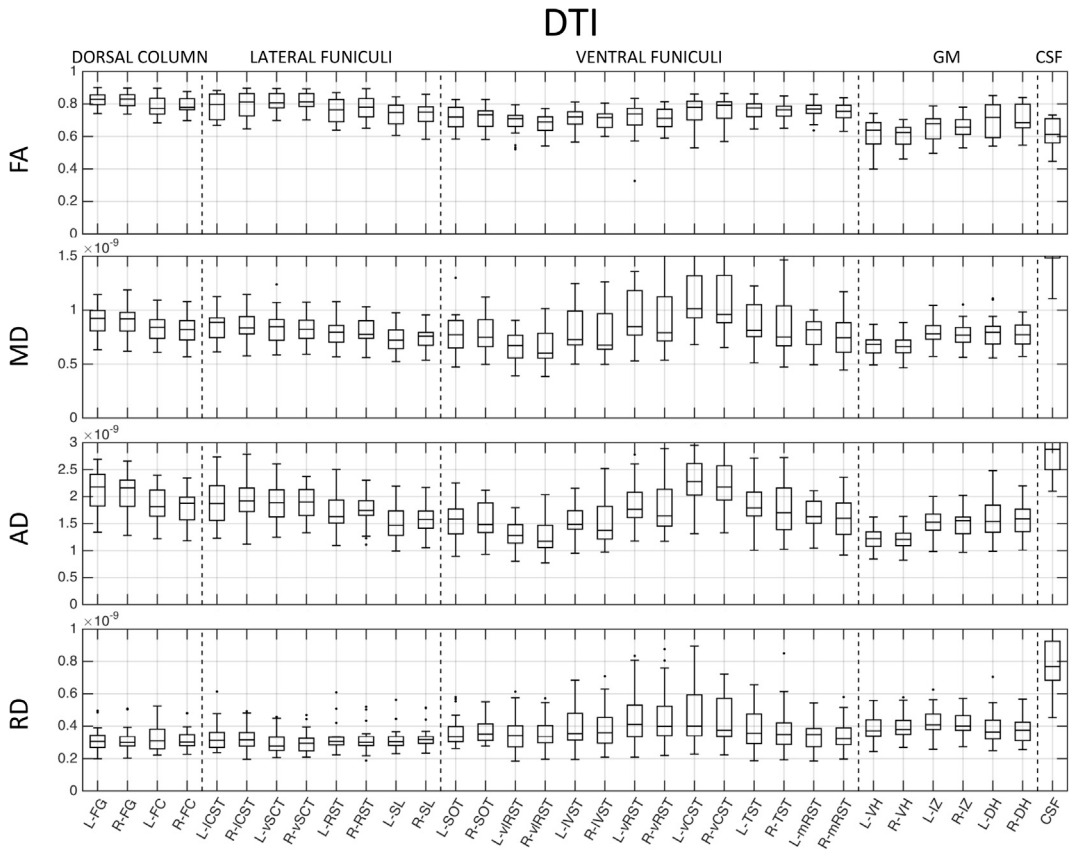


**Fig. 8.** Normative DTI values, averaged across 21 healthy subjects, for 33 regions of interest. ROIs are subdivided with vertical lines (from left to right) into dorsal column labels, lateral funiculi, ventral funiculi, GM, and CSF.

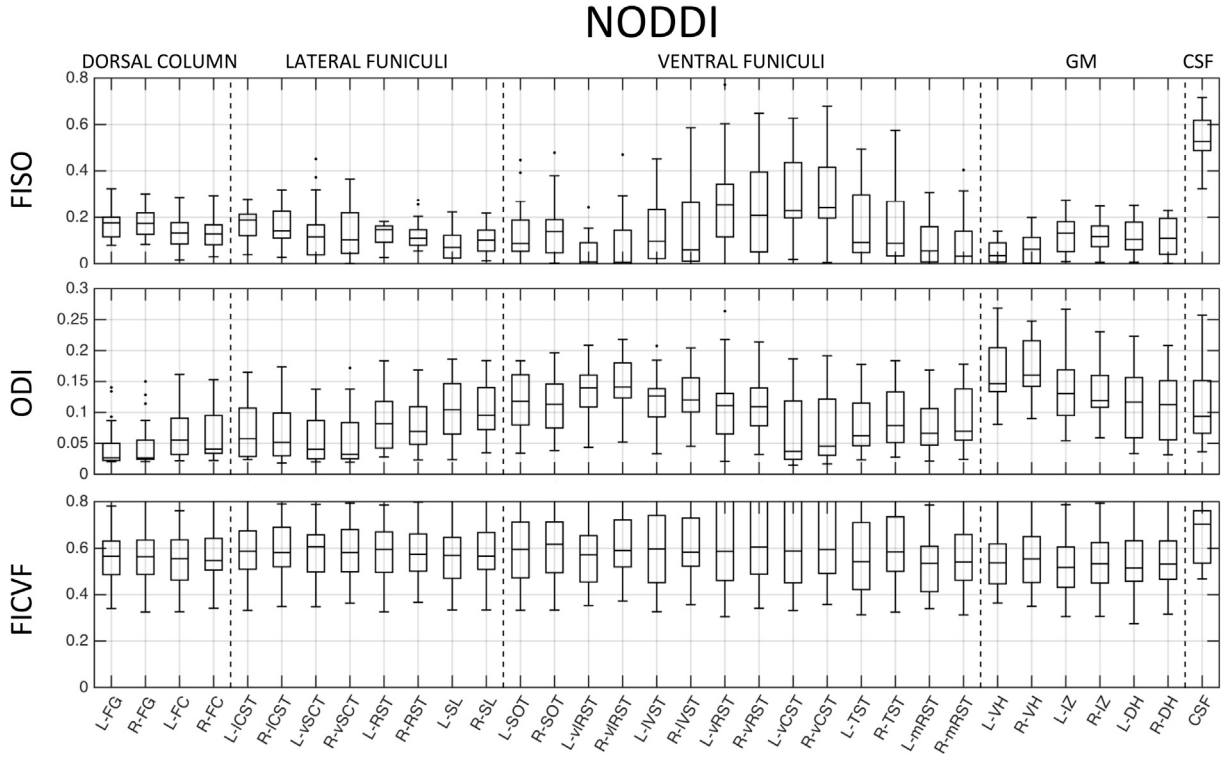


**Fig. 9.** Normative NODDI values, averaged across 21 healthy subjects, for 33 regions of interest. ROIs are subdivided with vertical lines (from left to right) into dorsal column labels, lateral funiculi, ventral funiculi, GM, and CSF.

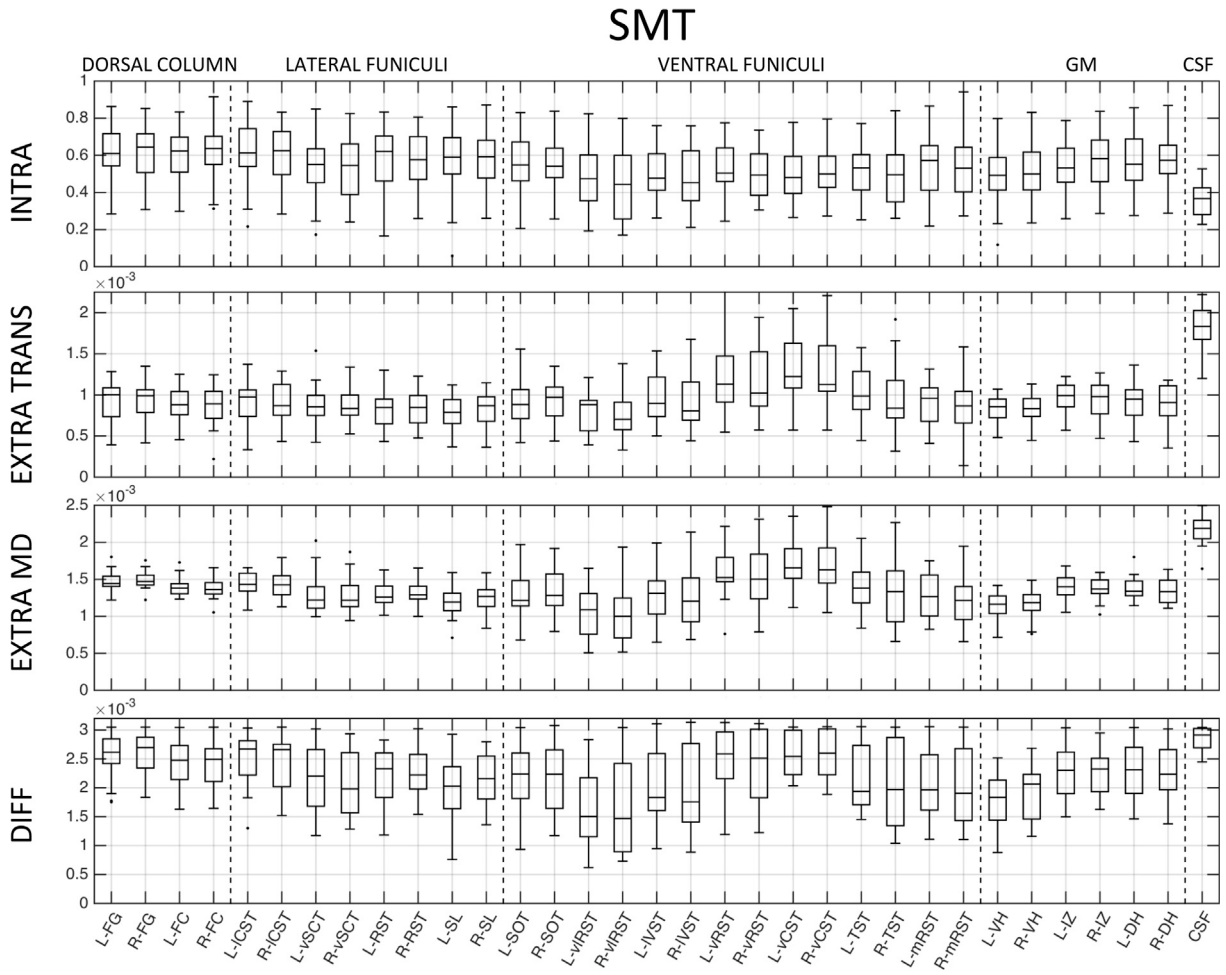


**Fig. 10.** Normative SMT values, averaged across 21 healthy subjects, for 33 regions of interest. ROIs are subdivided with vertical lines (from left to right) into dorsal column labels, lateral funiculi, ventral funiculi, GM, and CSF.

delineated, there is the ability to distinguish some microstructural environments.

We anticipate that the normative values (Figs. 8–10) should be useful when comparing healthy and patient populations as done for WM and GM in (By et al., 2017, 2018). Although not specific to any single microstructural environment, significant differences in quantitative metrics in specific tracts may provide more specific indices of disease progression or prognosis.

Correlations between histology and diffusion estimated microstructure provides insights into limitations of multi-compartment modeling. Most notably, the signal model (DTI) which makes no explicit assumptions on microstructure, showed strong correlations with all ground truth indices. The multi-compartment indices in which we expect strong correlations are the FICVF with the volume fraction of axons ($r = -0.15$) and INTRA with the same ($r = 0.18$), both of which showed non-significant correlations. Additionally, although not direct measurements, we expect additional diffusion measures to be sensitive to several microstructural measures. For example, the extra-cellular diffusivities would intuitively be inversely related to the density, diameter, and number of axons (i.e. more, big axons result in less extra-neurite space with more restrictions). We did find these trends, although with limited statistical significance. One interesting observation was the strong correlations with ODI. Ideally, ODI would be independent of axons diameters and densities, and only dependent on orientation, however this was not the case. ODI decreased with increasing density and volume fraction, possibly due to a higher packing of parallel axons. The explanation for a decrease in ODI with increasing axon diameter requires further investigation.

### 4.2. Limitations

There are a number of limitations to the current study. Most importantly, the histological analysis and template is based on a single adult human SC, whereas we compare these measures to diffusion-based metrics from a population of 21 adults, making direct one-to-one comparisons impossible. However, we simply aim to ask whether the diffusion models show expected trends, or correlate well with known anatomy. It is important to point out that this single-subject histological template shows anatomical variation that agrees with decades of previously published histological literature in human and animal models (Saliani et al., 2017). Thus, rather than expect exact quantification or correlation, we also ask whether the diffusion contrasts allow identification or separation of the expected microstructural environments. The second limitation could occur in registration to template space. Diffusion MRI is inherently SNR-limited, and spatial alignment may not be exact for all subjects, contributing to intra-subject variability. Additionally, tools for spinal cord pre-processing, normalization, and analysis are lacking in comparison to those of the brain, although several strides have been made with atlases, templates, and normalization tools. However, mis-registration in combination with expected anatomical variation, could lead to lower correlation that expected. Qualitatively (see montage Figs. 3–5), all subjects appear to be adequately registered and aligned.

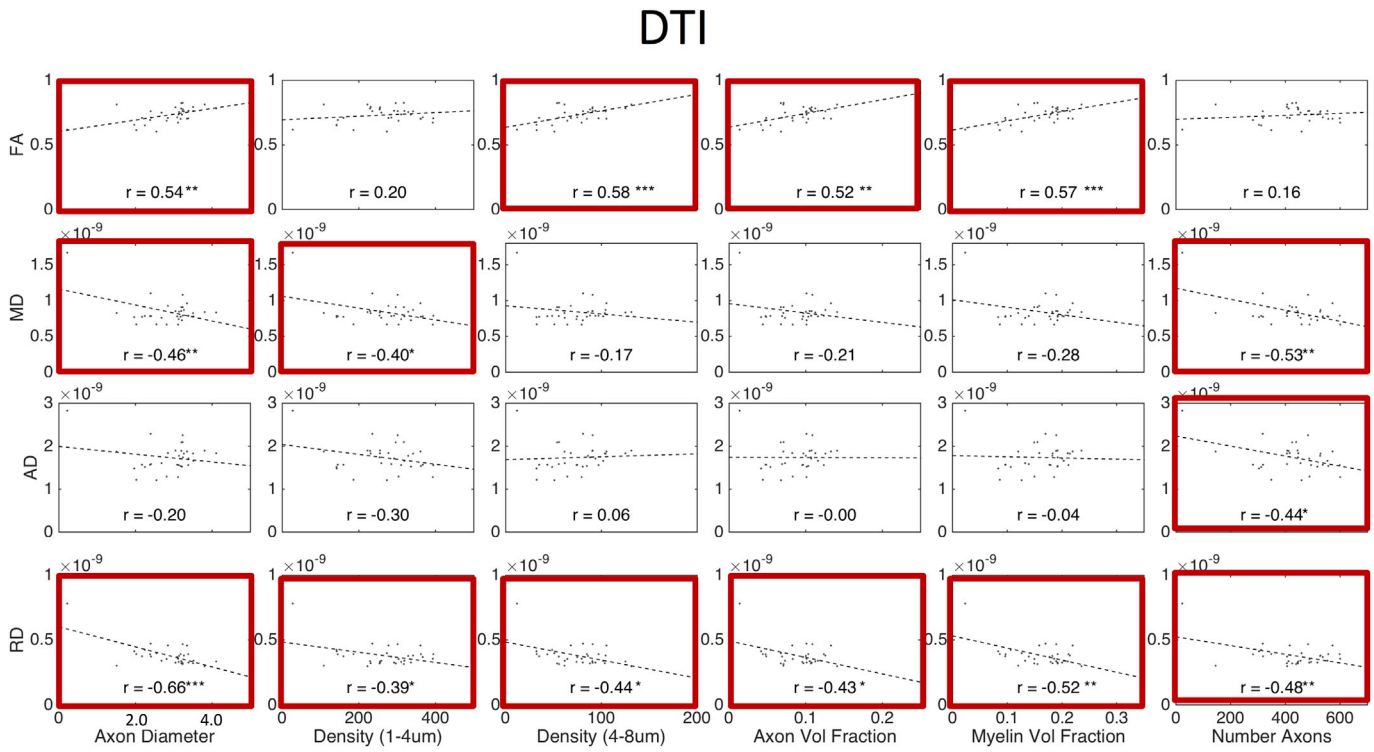


**Fig. 11.** Correlation between expected histological indices and DTI-derived metrics. Linear correlation coefficient is indicated in each sub-plot and statistical significance indicated by asterisk (*p < 0.05; **p < 0.01; ***p < 0.001) and bold plot outline. Histology and diffusion values are median values from histological template and diffusion population average, respectively.

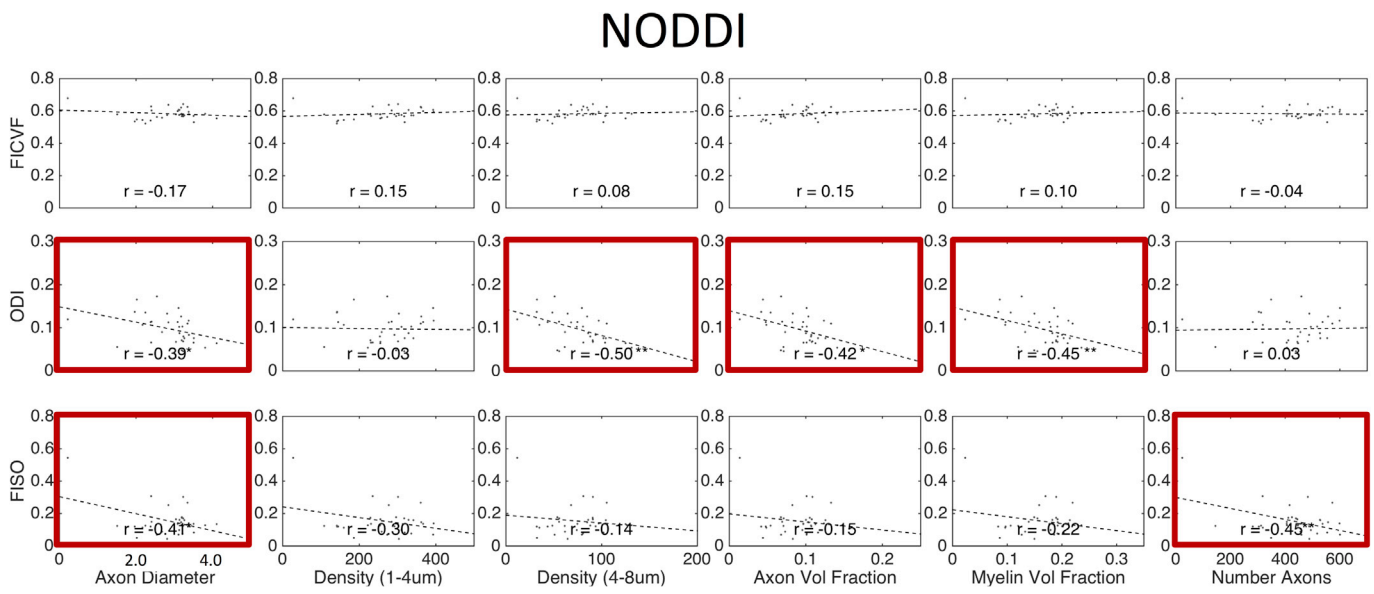


**Fig. 12.** Correlation between expected histological indices and NODDI-derived metrics. Linear correlation coefficient is indicated in each sub-plot and statistical significance indicated by asterisk (*p < 0.05; **p < 0.01; ***p < 0.001)) and bold plot outline. Histology and diffusion values are median values from histological template and diffusion population average, respectively.

Third, there is inherent variability in the spinal cord imaging data, as expected in spinal cord diffusion imaging (Grussu et al., 2015; By et al., 2017; By et al., 2018; Byet al., 2016; Grussuet al., 2019) – both due to noise and inherent inter-subject variations. This can cause possible inaccuracies in the derived metrics. As the imaging gets better, we expect accuracy and correlations to improve. Several experimental and design decisions could contribute to variability, including diffusion acquisition, registration algorithm utilized, metric extraction method, region of interest delineation. As discussed previously, the SC is composed of many small ROIs in both WM and GM, and partial volume effects contribute to both inter-subject variability and inter-ROI variability, particularly in small regions adjacent to the CSF.

Finally, the utilization of histology as a validation tool presents its own challenges, including choices of fixation procedures, myelin integrity preservation, staining limitations, and cutting/tissue preparation (see (Duvalet al., 2019) for a full discussion of limitations related to the

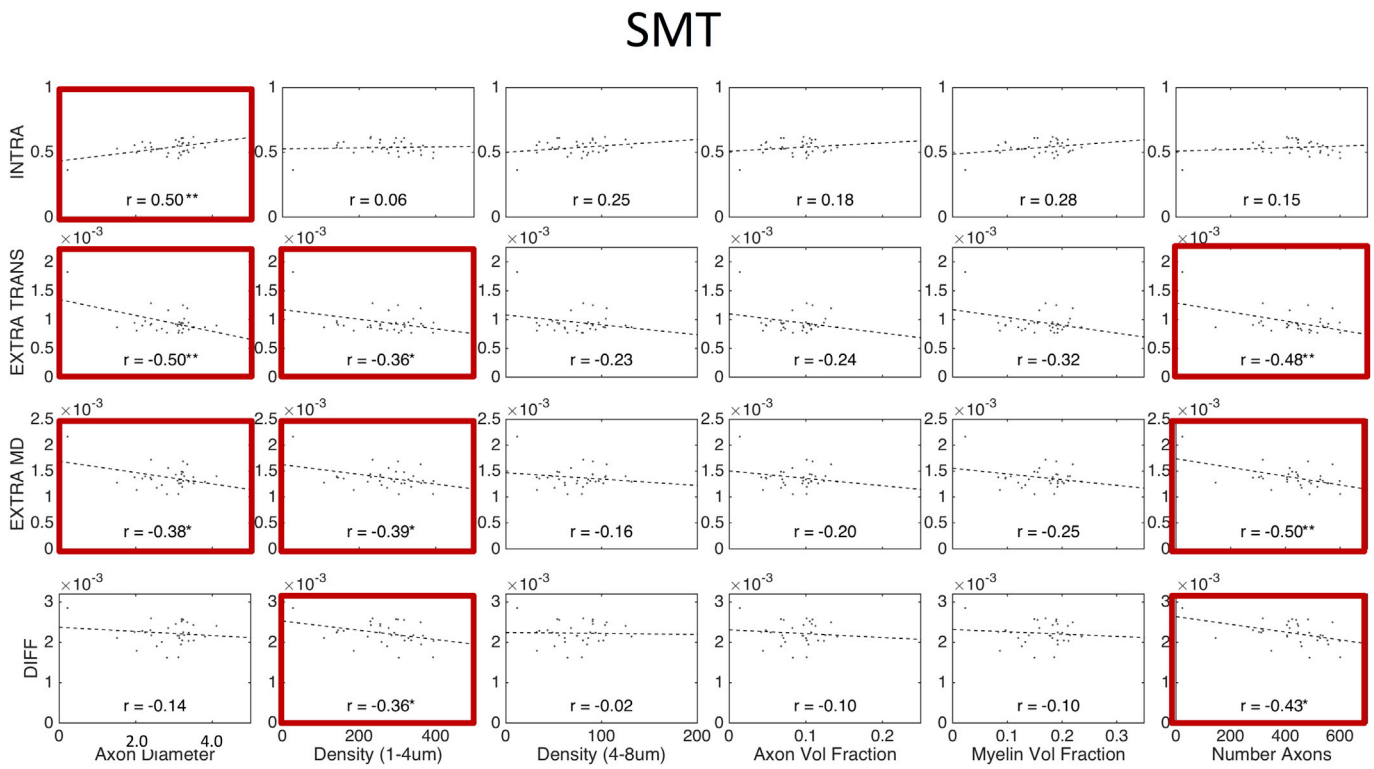


**Fig. 13.** Correlation between expected histological indices and SMT-derived metrics. Linear correlation coefficient is indicated in each sub-plot and statistical significance indicated by asterisk (*p < 0.05; **p < 0.01; ***p < 0.001)) and bold plot outline. Histology and diffusion values are median values from histological template and diffusion population average, respectively.

creation and quantification of the histological template). Together, these limitations may impact the magnitude and variance in all derived quantitative measures, as well as lead to biases (for example due to tissue shrinkage or lack of preservation). While biases and variation exist, the variation of microstructure within regions was shown to be less than that between regions (and less than that between various staining procedures) (Duvalet al., 2019), and it is important to re-emphasize that our analysis (ie., correlation analysis) simply ask whether these tissue or signal models are able to allow identification and separation of the expected trends in microstructural environments.

## 5. Conclusion

In this study, we apply advanced quantitative diffusion microstructural models to the human cervical spinal cord. We provide normative values of DTI, SMT, and NODDI indices in a number of WM ascending and descending pathways, as well as various GM regions. We then relate these measures to indices of the tissue microenvironment provided by a histological template. We find that DTI indices are sensitive to a number of microstructural features, but lack specificity. The multi-compartment modeling strategies, while sensitive to a number of microstructural features, do not capture the appropriate specific microstructural environment that are explicitly modelled. Although often regarded as a simple extension of the brain in the CNS, it may be necessary to re-envision diffusion microstructural models, or rely on pure signal models, to provide microstructure-sensitive contrast in the human SC.

## Acknowledgements

This work was supported by the National Institutes of Health under award numbers R21 NS087465-01, R01 EY023240, R01EB017230 and T32EB001628, by the National Multiple Sclerosis Society award number RG-1501-02840, the Department of Defense award number W81XWH-13-0073, and in part by the National Center for Research Resources grant UL1 RR024975-0.

## Appendix

### *Appendix A. Abbreviations*

All regions of interest have both a left (L) and right (R) label.

FG: fasciculus gracilis; FC: fasciculus cuneatus; lCST: lateral corticospinal tract; vSCT: ventral spinocerebellar tract; RST: rubrospinal tract; SL: spinal lemniscus (spinothalamic and spinoreticular tracts); SOT: spino-olivary tract; vlRST: ventrolateral reticulospinal tract; lVST: lateral vestibulospinal tract; vRST: ventral reticulospinal tract; vCST: ventral corticospinal tract; TST: tectospinal tract; mRST: medial reticulospinal tract; DH: dorsal horn; IZ: intermediate zone; VH: ventral horn; CSF: CSF contour.

### *Appendix B. Region grouping*

WM dorsal column: FG, FC.
WM lateral funiculi: lCST, vSCT, RST, SL.
WM ventral funiculi: SOT, vlRST, lVST, vRST, vCST, TST, mRST.
GM: VH, IZ, DH.
CSF: CSF.

## Appendix A. Supplementary data

Supplementary data to this article can be found online at https://doi.org/10.1016/j.neuroimage.2019.116026.

## References


Alexander, D.C., et al., Oct 1 2010. Orientationally invariant indices of axon diameter and density from diffusion MRI. Neuroimage 52 (4), 1374–1389. https://doi.org/10.1016/j.neuroimage.2010.05.043.

Araque Caballero, M.A., et al., Oct 1 2018. White matter diffusion alterations precede symptom onset in autosomal dominant Alzheimer's disease. Brain 141 (10), 3065–3080. https://doi.org/10.1093/brain/awy229.

Assaf, Y., Basser, P.J., Aug 1 2005. Composite hindered and restricted model of diffusion (CHARMED) MR imaging of the human brain. Neuroimage 27 (1), 48–58. https://doi.org/10.1016/j.neuroimage.2005.03.042.

Assaf, Y., Mayk, A., Cohen, Y., Nov 2000. Displacement imaging of spinal cord using q-space diffusion-weighted MRI. official journal of the Society of Magnetic Resonance in Medicine / Society of Magnetic Resonance in Medicine Magn. Reson. Med. 44 (5), 713–722.

Assaf, Y., Blumenfeld-Katzir, T., Yovel, Y., Basser, P.J., Jun 2008. AxCaliber: a method for measuring axon diameter distribution from diffusion MRI. official journal of the Society of Magnetic Resonance in Medicine / Society of Magnetic Resonance in Medicine Magn. Reson. Med. 59 (6), 1347–1354. https://doi.org/10.1002/mrm.21577.

Basser, P.J., Pierpaoli, C., Jun 1996. Microstructural and physiological features of tissues elucidated by quantitative-diffusion-tensor MRI. In: eng (Ed.), J. Magn. Reson., Ser. B 111 (3), 209–219.

Basser, P.J., Mattiello, J., LeBihan, D., Mar 1994. Estimation of the effective self-diffusion tensor from the NMR spin echo. J. Magn. Reson., Ser. B 103 (3), 247–254.

Battiston, M., et al., Apr 2018. Fast and reproducible in vivo T1 mapping of the human cervical spinal cord. official journal of the Society of Magnetic Resonance in Medicine / Society of Magnetic Resonance in Medicine Magn. Reson. Med. 79 (4), 2142–2148. https://doi.org/10.1002/mrm.26852.

Benjamini, D., Komlosh, M.E., Holtzclaw, L.A., Nevo, U., Basser, P.J., Apr 25 2016. White matter microstructure from nonparametric axon diameter distribution mapping. Neuroimage. https://doi.org/10.1016/j.neuroimage.2016.04.052.

Biton, I.E., Duncan, I.D., Cohen, Y., Feb 2006. High b-value q-space diffusion MRI in myelin-deficient rat spinal cords. Magn. Reson. Imag. 24 (2), 161–166. https://doi.org/10.1016/j.mri.2005.10.029.

Biton, I.E., Duncan, I.D., Cohen, Y., Nov 2007. q-Space diffusion of myelin-deficient spinal cords. official journal of the Society of Magnetic Resonance in Medicine / Society of Magnetic Resonance in Medicine Magn. Reson. Med. 58 (5), 993–1000. https://doi.org/10.1002/mrm.21389.

Budde, M.D., Annese, J., 2013. Quantification of anisotropy and fiber orientation in human brain histological sections. Front. Integr. Neurosci. 7, 3. https://doi.org/10.3389/fnint.2013.00003.

Budde, M.D., Frank, J.A., Oct 15 2012. Examining brain microstructure using structure tensor analysis of histological sections. *NeuroImage,* Research Support, N.I.H., Intramural Research Support, Non-U.S. Gov't, 63, 1–10. https://doi.org/10.1016/j.neuroimage.2012.06.042, 1.

Budde, M.D., Xie, M., Cross, A.H., Song, S.K., Mar 4 2009. Axial diffusivity is the primary correlate of axonal injury in the experimental autoimmune encephalomyelitis spinal cord: a quantitative pixelwise analysis. J. Neurosci. 29 (9), 2805–2813. https://doi.org/10.1523/JNEUROSCI.4605-08.2009.

By, S., Xu, J., Box, B.A., Bagnato, F.R., Smith, S.A., 2017. Application and evaluation of NODDI in the cervical spinal cord of multiple sclerosis patients. Neuroimage Clin. 15, 333–342. https://doi.org/10.1016/j.nicl.2017.05.010.

By, S., Xu, J., Box, B.A., Bagnato, F.R., Smith, S.A., Apr 2018. Multi-compartmental diffusion characterization of the human cervical spinal cord in vivo using the spherical mean technique. NMR Biomed. 31 (4), e3894 https://doi.org/10.1002/nbm.3894.

By, S., et al., Dec 2016. Quantifying the impact of underlying measurement error on cervical spinal cord diffusion tensor imaging at 3T. J. Magn. Reson. Imaging : JMRI 44 (6), 1608–1618. https://doi.org/10.1002/jmri.25308.

Calamante, F., Tournier, J.D., Jackson, G.D., Connelly, A., Dec 2010. Track-density imaging (TDI): super-resolution white matter imaging using whole-brain track-density mapping. Neuroimage 53 (4), 1233–1243. https://doi.org/10.1016/j.neuroimage.2010.07.024.

Carpenter, M.B., 1991. Spinal cord: gross anatomy and internal structure. In: Core Text of Neuroanatomy, vol. 1. Williams & Wilkins, Baltimore, MD, pp. 57–82.

Carpenter, M.B., 1991. Tracts of the spinal cord. In: Core Text of Neuroanatomy, vol. 1. Williams & Wilkins, Baltimore, MD, pp. 83–114.

Chen, L.M., Mishra, A., Yang, P.F., Wang, F., Gore, J.C., May 12 2015. Injury alters intrinsic functional connectivity within the primate spinal cord. Proc. Natl. Acad. Sci. U. S. A 112 (19), 5991–5996. https://doi.org/10.1073/pnas.1424106112.

Chevis, C.F., et al., Feb 2013. Spinal cord atrophy correlates with disability in Friedreich's ataxia. Cerebellum 12 (1), 43–47. https://doi.org/10.1007/s12311-012-0390-6.

Claus, E.B., et al., Feb 2010. Defining future directions in spinal cord tumor research: proceedings from the National Institutes of Health workshop. J. Neurosurg. Spine 12 (2), 117–121. https://doi.org/10.3171/2009.7.SPINE09137.

Clowry, G.J., 2007. The dependence of spinal cord development on corticospinal input and its significance in understanding and treating spastic cerebral palsy. Neurosci. Biobehav. Rev. 31 (8), 1114–1124. https://doi.org/10.1016/j.neubiorev.2007.04.007.

Cohen-Adad, J., Nov 15 2018. Microstructural imaging in the spinal cord and validation strategies. Neuroimage 182, 169–183. https://doi.org/10.1016/j.neuroimage.2018.04.009.

De Leener, B., Fonov, V.S., Collins, D.L., Callot, V., Stikov, N., Cohen-Adad, J., Jan 15 2018. PAM50: unbiased multimodal template of the brainstem and spinal cord aligned with the ICBM152 space. Neuroimage 165, 170–179. https://doi.org/10.1016/j.neuroimage.2017.10.041.

De Leener, B., et al., Jan 15 2017. SCT: spinal Cord Toolbox, an open-source software for processing spinal cord MRI data. Neuroimage 145, 24–43. https://doi.org/10.1016/j.neuroimage.2016.10.009. Pt A.

De Santis, S., et al., Apr 7 2018. Characterizing microstructural tissue properties in multiple sclerosis with diffusion MRI at 7T and 3T: the impact of the experimental design. Neuroscience. https://doi.org/10.1016/j.neuroscience.2018.03.048.

DeBoy, C.A., et al., Aug 2007. High resolution diffusion tensor imaging of axonal damage in focal inflammatory and demyelinating lesions in rat spinal cord. Brain 130 (Pt 8), 2199–2210. https://doi.org/10.1093/brain/awm122.

Dula, A.N., Gochberg, D.F., Valentine, H.L., Valentine, W.M., Does, M.D., Apr 2010. Multiexponential T2, magnetization transfer, and quantitative histology in white matter tracts of rat spinal cord. official journal of the Society of Magnetic Resonance in Medicine / Society of Magnetic Resonance in Medicine Magn. Reson. Med. 63 (4), 902–909. https://doi.org/10.1002/mrm.22267.

Duval, T., Smith, V., Stikov, N., Klawiter, E.C., Cohen-Adad, J., May 2018. Scan-rescan of axcaliber, macromolecular tissue volume, and g-ratio in the spinal cord. official journal of the Society of Magnetic Resonance in Medicine / Society of Magnetic Resonance in Medicine Magn. Reson. Med. 79 (5), 2759–2765. https://doi.org/10.1002/mrm.26945.

Duval, T., et al., Sep 2015. In vivo mapping of human spinal cord microstructure at 300mT/m. Neuroimage 118, 494–507. https://doi.org/10.1016/j.neuroimage.2015.06.038 (in eng).

Duval, T., et al., Jan 15 2017. g-Ratio weighted imaging of the human spinal cord in vivo. Neuroimage 145, 11–23. https://doi.org/10.1016/j.neuroimage.2016.09.018. Pt A.

Duval, T., et al., Jan 15 2019. Axons morphometry in the human spinal cord. Neuroimage 185, 119–128. https://doi.org/10.1016/j.neuroimage.2018.10.033.

Dyrby, T.B., Sogaard, L.V., Hall, M.G., Ptito, M., Alexander, D.C., Sep 28 2012. Contrast and stability of the axon diameter index from microstructure imaging with diffusion MRI. official journal of the Society of Magnetic Resonance in Medicine / Society of Magnetic Resonance in Medicine Magn. Reson. Med.. https://doi.org/10.1002/mrm.24501.

Dyrby, T.B., Sogaard, L.V., Hall, M.G., Ptito, M., Alexander, D.C., Sep 2013. Contrast and stability of the axon diameter index from microstructure imaging with diffusion MRI. official journal of the Society of Magnetic Resonance in Medicine / Society of Magnetic Resonance in Medicine Magn. Reson. Med. 70 (3), 711–721. https://doi.org/10.1002/mrm.24501.

Dyrby, T.B., Innocenti, G., Bech, M., Lundell, H., Jun 16 2018. Validation strategies for the interpretation of microstructure imaging using diffusion MRI. Neuroimage. https://doi.org/10.1016/j.neuroimage.2018.06.049.

Fan, Q., et al., Jan 12 2018. Validation of diffusion MRI estimates of compartment size and volume fraction in a biomimetic brain phantom using a human MRI scanner with 300mT/m maximum gradient strength. Neuroimage. https://doi.org/10.1016/j.neuroimage.2018.01.004.

Felten, D.L., Shetty, A.N., Felten, D.L., 2010. In: Netter's Atlas of Neuroscience, second ed. Saunders/Elsevier, Philadelphia, PA, p. 438. xviii.

Felten, D.L., O'Banion, M.K., Maida, M.S., Netter, F.H., 2016. In: Netter's Atlas of Neuroscience, third ed. Elsevier, Philadelphia, PA, p. 477. xvii.

Ferizi, U., et al., Sep 2015. White matter compartment models for in vivo diffusion MRI at 300mT/m. Neuroimage 118, 468–483. https://doi.org/10.1016/j.neuroimage.2015.06.027.

Fieremans, E., Lee, H.H., Jun 18 2018. Physical and numerical phantoms for the validation of brain microstructural MRI: a cookbook. Neuroimage. https://doi.org/10.1016/j.neuroimage.2018.06.046.

Fieremans, E., De Deene, Y., Delputte, S., Ozdemir, M.S., Achten, E., Lemahieu, I., Oct 7 2008. The design of anisotropic diffusion phantoms for the validation of diffusion weighted magnetic resonance imaging. Phys. Med. Biol. 53 (19), 5405–5419. https://doi.org/10.1088/0031-9155/53/19/009.

Fujiyoshi, K., et al., Apr 2013. Diffusion tensor imaging and tractography of the spinal cord: from experimental studies to clinical application. Exp. Neurol. 242, 74–82. https://doi.org/10.1016/j.expneurol.2012.07.015.

Ganzetti, M., Wenderoth, N., Mantini, D., 2014. Whole brain myelin mapping using T1- and T2-weighted MR imaging data. Front. Hum. Neurosci. 8, 671. https://doi.org/10.3389/fnhum.2014.00671.

Garyfallidis, E., et al., Apr 15 2018. Recognition of white matter bundles using local and global streamline-based registration and clustering. Neuroimage 170, 283–295. https://doi.org/10.1016/j.neuroimage.2017.07.015.

Grussu, F., Schneider, T., Zhang, H., Alexander, D.C., Wheeler-Kingshott, C.A., May 1 2015. Neurite orientation dispersion and density imaging of the healthy cervical spinal cord in vivo. Neuroimage 111, 590–601. https://doi.org/10.1016/j.neuroimage.2015.01.045.

Grussu, F., et al., 2016. A framework for optimal whole-sample histological quantification of neurite orientation dispersion in the human spinal cord. J. Neurosci. Methods 273 (11), 20–32. https://doi.org/10.1016/j.jneumeth.2016.08.002 in eng.

Grussu, F., et al., Sep 2017. Neurite dispersion: a new marker of multiple sclerosis spinal cord pathology? Ann. Clin. Transl. Neurol. 4 (9), 663–679. https://doi.org/10.1002/acn3.445.

Grussu, F., et al., Feb 2019. Relevance of time-dependence for clinically viable diffusion imaging of the spinal cord. Magn. Reson. Med. 81 (2), 1247–1264. https://doi.org/10.1002/mrm.27463 (in eng).

Guo, Y., et al., 2019. White matter microstructure alterations in patients with spinal cord injury assessed by diffusion tensor imaging. Front. Hum. Neurosci. https://doi.org/10.3389/fnhum.2019.00011.

Harkins, K.D., Dula, A.N., Does, M.D., Mar 2012. Effect of intercompartmental water exchange on the apparent myelin water fraction in multiexponential T2

measurements of rat spinal cord. official journal of the Society of Magnetic Resonance in Medicine / Society of Magnetic Resonance in Medicine Magn. Reson. Med. 67 (3), 793–800. https://doi.org/10.1002/mrm.23053.
Harkins, K.D., Valentine, W.M., Gochberg, D.F., Does, M.D., 2013. In-vivo multi-exponential T2, magnetization transfer and quantitative histology in a rat model of intramyelinic edema. Neuroimage Clin. 2, 810–817. https://doi.org/10.1016/j.nicl.2013.06.007.
Hasan, K.M., Eluvathingal, T.J., Kramer, L.A., Ewing-Cobbs, L., Dennis, M., Fletcher, J.M., Apr 2008. White matter microstructural abnormalities in children with spina bifida myelomeningocele and hydrocephalus: a diffusion tensor tractography study of the association pathways. J. Magn. Reson. Imaging : JMRI 27 (4), 700–709. https://doi.org/10.1002/jmri.21297.
Hubbard, P.L., Zhou, F.L., Eichhorn, S.J., Parker, G.J., Jan 27 2014. Biomimetic phantom for the validation of diffusion magnetic resonance imaging. official journal of the Society of Magnetic Resonance in Medicine / Society of Magnetic Resonance in Medicine Magn. Reson. Med.. https://doi.org/10.1002/mrm.25107.
Jelescu, I.O., Budde, M.D., Nov 2017. Design and validation of diffusion MRI models of white matter. Front. Physiol. 28 https://doi.org/10.3389/fphy.2017.00061.
Jelescu, I.O., Veraart, J., Adisetiyo, V., Milla, S.S., Novikov, D.S., Fieremans, E., Feb 15 2015. One diffusion acquisition and different white matter models: how does microstructure change in human early development based on WMTI and NODDI? Neuroimage 107, 242–256. https://doi.org/10.1016/j.neuroimage.2014.12.009.
Jespersen, S.N., Olesen, J.L., Hansen, B., Shemesh, N., Nov 15 2018. Diffusion time dependence of microstructural parameters in fixed spinal cord. Neuroimage 182, 329–342. https://doi.org/10.1016/j.neuroimage.2017.08.039.
Kaden, E., Kelm, N.D., Carson, R.P., Does, M.D., Alexander, D.C., Oct 1 2016. Multi-compartment microscopic diffusion imaging. Neuroimage 139, 346–359. https://doi.org/10.1016/j.neuroimage.2016.06.002.
Kadota, Y., et al., Nov 12 2018. Differentiation between glioblastoma and solitary brain metastasis using neurite orientation dispersion and density imaging. J. Neuroradiol. https://doi.org/10.1016/j.neurad.2018.10.005.
Kamiya, K., et al., Jul 2018. Diffusional kurtosis imaging and white matter microstructure modeling in a clinical study of major depressive disorder. NMR Biomed. 31 (7), e3938. https://doi.org/10.1002/nbm.3938.
Kawamata, T., Akiyama, H., Yamada, T., McGeer, P.L., Mar 1992. Immunologic reactions in amyotrophic lateral sclerosis brain and spinal cord tissue. Am. J. Pathol. 140 (3), 691–707.
Klawiter, E.C., et al., Apr 15 2011. Radial diffusivity predicts demyelination in ex vivo multiple sclerosis spinal cords. Neuroimage 55 (4), 1454–1460. https://doi.org/10.1016/j.neuroimage.2011.01.007.
Krishnan, C., Kaplin, A.I., Pardo, C.A., Kerr, D.A., Keswani, S.C., May 2006. Demyelinating disorders: update on transverse myelitis. Curr. Neurol. Neurosci. Rep. 6 (3), 236–243.
Kuczynski, A.M., et al., Nov 29 2017. Corticospinal tract diffusion properties and robotic visually guided reaching in children with hemiparetic cerebral palsy. Hum. Brain Mapp. https://doi.org/10.1002/hbm.23904.
Landman, B.A., Farrell, J.A., Smith, S.A., Reich, D.S., Calabresi, P.A., van Zijl, P.C., Feb 2010. Complex geometric models of diffusion and relaxation in healthy and damaged white matter. NMR Biomed. 23 (2), 152–162. https://doi.org/10.1002/nbm.1437.
Lee, H.-H., Fieremans, E., Novikov, D.S., 2018. What dominates the time dependence of diffusion transverse to axons: intra- or extra-axonal water? Neuroimage 182, 500–510, 2018/11/15/. https://doi.org/10.1016/j.neuroimage.2017.12.038.
Leergaard, T.B., et al., 2010. Quantitative histological validation of diffusion MRI fiber orientation distributions in the rat brain. PLoS One 5 (1), e8595. https://doi.org/10.1371/journal.pone.0008595.
Lema, A., et al., Mar 2017. A comparison of magnetization transfer methods to assess brain and cervical cord microstructure in multiple sclerosis. J. Neuroimaging 27 (2), 221–226. https://doi.org/10.1111/jon.12377.
Lévy, S., Benhamou, M., Naaman, C., Rainville, P., Callot, V., Cohen-Adad, J., Oct 2015. White matter atlas of the human spinal cord with estimation of partial volume effect. Neuroimage 119, 262–271. https://doi.org/10.1016/j.neuroimage.2015.06.040 eng.
Levy, S., et al., 2018. Test-retest reliability of myelin imaging in the human spinal cord: measurement errors versus region- and aging-induced variations. PLoS One 13 (1), e0189944. https://doi.org/10.1371/journal.pone.0189944.
Li, H., Chow, H.M., Chugani, D.C., Chugani, H.T., Dec 2018. Minimal number of gradient directions for robust measurement of spherical mean diffusion weighted signal. Magn. Reson. Imag. 54, 148–152. https://doi.org/10.1016/j.mri.2018.08.020.
Li, H., Chow, H.M., Chugani, D.C., Chugani, H.T., Apr 2019. Linking spherical mean diffusion weighted signal with intra-axonal volume fraction. Magn. Reson. Imag. 57, 75–82. https://doi.org/10.1016/j.mri.2018.11.006.
Ljungberg, E., et al., Oct 2017. Rapid myelin water imaging in human cervical spinal cord. official journal of the Society of Magnetic Resonance in Medicine / Society of Magnetic Resonance in Medicine Magn. Reson. Med. 78 (4), 1482–1487. https://doi.org/10.1002/mrm.26551.
Martin, A.R., et al., 2018. Can microstructural MRI detect subclinical tissue injury in subjects with asymptomatic cervical spinal cord compression? A prospective cohort study. BMJ Open 8 (4), e019809. https://doi.org/10.1136/bmjopen-2017-019809.
Mascalchi, M., Salvi, F., Piacentini, S., Bartolozzi, C., Jul 1994. Friedreich's ataxia: MR findings involving the cervical portion of the spinal cord. AJR Am. J. Roentgenol. 163 (1), 187–191. https://doi.org/10.2214/ajr.163.1.8010211.
Masjoodi, S., Hashemi, H., Oghabian, M.A., Sharifi, G., Sep 2018. Differentiation of edematous, tumoral and normal areas of brain using diffusion tensor and neurite orientation dispersion and density imaging. J. Biomed. Phys. Eng. 8 (3), 251–260.
Metzler-Baddeley, C., et al., Jan 31 2019. Fornix white matter glia damage causes hippocampal gray matter damage during age-dependent limbic decline. Sci. Rep. 9 (1), 1060. https://doi.org/10.1038/s41598-018-37658-5.
Niu, J., et al., Nov 2013. Modality-based organization of ascending somatosensory axons in the direct dorsal column pathway. In: eng (Ed.), J. Neurosci. 33 (45), 17691–17709. https://doi.org/10.1523/JNEUROSCI.3429-13.2013.
Nossin-Manor, R., Duvdevani, R., Cohen, Y., Apr 2002. q-Space high b value diffusion MRI of hemi-crush in rat spinal cord: evidence for spontaneous regeneration. Magn. Reson. Imag. 20 (3), 231–241.
Novikov, D.S., Fieremans, E., Jespersen, S.N., Kiselev, V.G., Oct 15 2018. Quantifying brain microstructure with diffusion MRI: theory and parameter estimation. In: NMR in Biomedicine, p. e3998. https://doi.org/10.1002/nbm.3998.
Novikov, D.S., Kiselev, V.G., Jespersen, S.N., Jun 2018. On modeling. official journal of the Society of Magnetic Resonance in Medicine / Society of Magnetic Resonance in Medicine Magn. Reson. Med. 79 (6), 3172–3193. https://doi.org/10.1002/mrm.27101.
Ong, H.H., Wehrli, F.W., Jul 2010. Quantifying axon diameter and intra-cellular volume fraction in excised mouse spinal cord with q-space imaging. In: eng (Ed.), Neuroimage 51 (4), 1360–1366. https://doi.org/10.1016/j.neuroimage.2010.03.063.
Panagiotaki, E., Schneider, T., Siow, B., Hall, M.G., Lythgoe, M.F., Alexander, D.C., Feb 1 2012. Compartment models of the diffusion MR signal in brain white matter: a taxonomy and comparison. Neuroimage 59 (3), 2241–2254. https://doi.org/10.1016/j.neuroimage.2011.09.081.
Parvathaneni, P., et al., Jul 2018. Empirical reproducibility, sensitivity, and optimization of acquisition protocol, for Neurite Orientation Dispersion and Density Imaging using AMICO. Magn. Reson. Imag. 50, 96–109. https://doi.org/10.1016/j.mri.2018.03.004.
Pierpaoli, C., Jezzard, P., Basser, P.J., Barnett, A., Chiro, G.D., December 1996 1996. Diffusion tensor MR imaging of the human brain. Radiology 201, 637–648.
Pietsch, M., et al., Feb 1 2019. A framework for multi-component analysis of diffusion MRI data over the neonatal period. Neuroimage 186, 321–337. https://doi.org/10.1016/j.neuroimage.2018.10.060.
Reich, D.S., et al., Nov 1 2007. Multiparametric magnetic resonance imaging analysis of the corticospinal tract in multiple sclerosis. Neuroimage 38 (2), 271–279. https://doi.org/10.1016/j.neuroimage.2007.07.049.
Saliani, A., Perraud, B., Duval, T., Stikov, N., Rossignol, S., Cohen-Adad, J., 2017. Axon and myelin morphology in animal and human spinal cord. Front. Neuroanat. 11, 129. https://doi.org/10.3389/fnana.2017.00129.
Samson, R.S., et al., Dec 2013. Tissue- and column-specific measurements from multi-parameter mapping of the human cervical spinal cord at 3 T. NMR Biomed. 26 (12), 1823–1830. https://doi.org/10.1002/nbm.3022.
Scherrer, B., Schwartzman, A., Taquet, M., Sahin, M., Prabhu, S.P., Warfield, S.K., Sep 2016. Characterizing brain tissue by assessment of the distribution of anisotropic microstructural environments in diffusion-compartment imaging (DIAMOND). official journal of the Society of Magnetic Resonance in Medicine / Society of Magnetic Resonance in Medicine Magn. Reson. Med. 76 (3), 963–977. https://doi.org/10.1002/mrm.25912.
Schilling, K., Janve, V., Gao, Y., Stepniewska, I., Landman, B.A., Anderson, A.W., Apr 1 2016. Comparison of 3D orientation distribution functions measured with confocal microscopy and diffusion MRI. Neuroimage 129, 185–197. https://doi.org/10.1016/j.neuroimage.2016.01.022.
Schilling, K.G., Janve, V., Gao, Y., Stepniewska, I., Landman, B.A., Anderson, A.W., Jan 15 2018. Histological validation of diffusion MRI fiber orientation distributions and dispersion. Neuroimage 165, 200–221. https://doi.org/10.1016/j.neuroimage.2017.10.046.
Schilling, K.G., et al., Oct 11 2018. Limits to anatomical accuracy of diffusion tractography using modern approaches. Neuroimage 185, 1–11. https://doi.org/10.1016/j.neuroimage.2018.10.029.
Schilling, K., et al., 2018. Anatomically-informed and patient-specific diffusion tensor sampling schemes for the cervical spinal cord. In: Proceedings of the International Society of Magnetic Resonance in Medicine, vol. 26. France, Paris.
Schwartz, E.D., et al., Jan 19 2005. MRI diffusion coefficients in spinal cord correlate with axon morphometry. Neuroreport 16 (1), 73–76.
Seehaus, A., et al., 2015. Histological validation of high-resolution DTI in human post mortem tissue. Front. Neuroanat. 9, 98. https://doi.org/10.3389/fnana.2015.00098.
Skinner, N.P., Kurpad, S.N., Schmit, B.D., Tugan Muftuler, L., Budde, M.D., Apr 2017. Rapid in vivo detection of rat spinal cord injury with double-diffusion-encoded magnetic resonance spectroscopy. official journal of the Society of Magnetic Resonance in Medicine / Society of Magnetic Resonance in Medicine Magn. Reson. Med. 77 (4), 1639–1649. https://doi.org/10.1002/mrm.26243.
Smith, A.K., Dortch, R.D., Dethrage, L.M., Smith, S.A., Jul 15 2014. Rapid, high-resolution quantitative magnetization transfer MRI of the human spinal cord. Neuroimage 95, 106–116. https://doi.org/10.1016/j.neuroimage.2014.03.005.
Sone, D., Sato, N., Ota, M., Maikusa, N., Kimura, Y., Matsuda, H., 2018. Abnormal neurite density and orientation dispersion in unilateral temporal lobe epilepsy detected by advanced diffusion imaging. Neuroimage Clin. 20, 772–782. https://doi.org/10.1016/j.nicl.2018.09.017.
Song, S.K., et al., May 15 2005. Demyelination increases radial diffusivity in corpus callosum of mouse brain. Neuroimage 26 (1), 132–140. https://doi.org/10.1016/j.neuroimage.2005.01.028.
Spano, B., et al., Nov 2018. Disruption of neurite morphology parallels MS progression. Neurol. Neuroimmunol. Neuroinflamm. 5 (6), e502 https://doi.org/10.1212/NXI.0000000000000502.
Stadelmann, C., 2011. Multiple sclerosis as a neurodegenerative disease: pathology, mechanisms and therapeutic implications. Curr. Opin. Neurol. 24 (3), 224–229. https://doi.org/10.1097/WCO.0b013e328346056f.
Wang, Y., et al., Dec 2011. Quantification of increased cellularity during inflammatory demyelination. Brain 134 (12), 3590–3601. https://doi.org/10.1093/brain/awr307.

Westin, C.F., et al., Jul 15 2016. Q-space trajectory imaging for multidimensional diffusion MRI of the human brain. Neuroimage 135, 345–362. https://doi.org/10.1016/j.neuroimage.2016.02.039.

Wheeler-Kingshott, C.A., et al., May 2002. Investigating cervical spinal cord structure using axial diffusion tensor imaging. Neuroimage 16 (1), 93–102. https://doi.org/10.1006/nimg.2001.1022.

Wilm, B.J., Svensson, J., Henning, A., Pruessmann, K.P., Boesiger, P., Kollias, S.S., Mar 2007. Reduced field-of-view MRI using outer volume suppression for spinal cord diffusion imaging. official journal of the Society of Magnetic Resonance in Medicine / Society of Magnetic Resonance in Medicine Magn. Reson. Med. 57 (3), 625–630. https://doi.org/10.1002/mrm.21167.

Xu, J., et al., Feb 15 2013. Improved in vivo diffusion tensor imaging of human cervical spinal cord. Neuroimage 67, 64–76. https://doi.org/10.1016/j.neuroimage.2012.11.014.

Xu, J., et al., Dec 2014. Mapping mean axon diameter and axonal volume fraction by MRI using temporal diffusion spectroscopy. Neuroimage 103, 10–19. https://doi.org/10.1016/j.neuroimage.2014.09.006.

Xu, J., et al., Apr 2016. Fast and simplified mapping of mean axon diameter using temporal diffusion spectroscopy. NMR Biomed. 29 (4), 400–410.

Zhang, H., Schneider, T., Wheeler-Kingshott, C.A., Alexander, D.C., Jul 16 2012. NODDI: Practical in vivo neurite orientation dispersion and density imaging of the human brain. Research Support, Non-U.S. Gov't vol Neuroimage 61 (4), 1000–1016. https://doi.org/10.1016/j.neuroimage.2012.03.072.